NASA TECHNICAL TRANSLATION

NASA TT F-723

SATELLITE CLIMATOLOGY

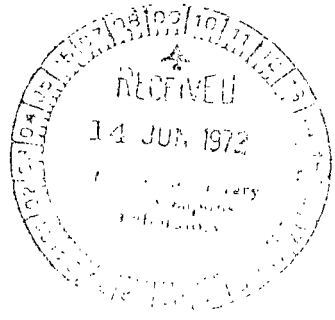

by K. Ya. Kondrat'yev

"Hydrometeorological" Press,
Leningrad, 1971

NATIONAL AERONAUTICS AND SPACE ADMINISTRATION • WASHINGTON, D. C. • JUNE 1972

NASA TT F-723

SATELLITE CLIMATOLOGY

By K. Ya. Kondrat'yev

Translation of "Sputnikova Klimatologiya."
"Hydrometeorological" Press,
Leningrad, 1971

NATIONAL AERONAUTICS AND SPACE ADMINISTRATION

For sale by the National Technical Information Service, Springfield, Virginia 22151
$3.00

TABLE OF CONTENTS /65

SATELLITE CLIMATOLOGY

K. Ya. Kondrat'yev

ABSTRACT. The successful functioning of meteorological space systems in the USSR and USA has resulted in a situation where the volume of satellite meteorological information exceeds by far the volume of all the usual meteorological data accumulated during many decades. The gigantic amount of data from satellite meteorological observations and their global nature have introduced the problem of utilizing all these data for climatological investigations. First of all a generalization has been undertaken of the results of similar investigations in the area of satellite climatology. The problem of the classification of cloudiness on the basis of satellite data and the regularities of the planetary distributions of cloud cover have been discussed thoroughly. The possibilities of working out semiempirical procedures have been discussed for determining the fields of temperature, moisture content, precipitation, vertical motions, and the distribution of snow and ice covers on the basis of utilizing television and infrared information and also on the basis of information about the emergent radiation fields in various regions of the spectra. The distinctive features of the spatial-temporal variability of the global radiation balance of the Earth-atmosphere system and its components are analyzed in detail. A comparison of the data of the experimental and computational radiation climatology of the Earth is made.

This book may be of interest to a broad group of specialists in the area of meteorology and atmospheric physics for space research, and also for graduate students and students in advanced courses of the corresponding specialties.

INTRODUCTION

The abundance of meteorological data obtained with the help of the /3* numerous ground-based weather stations has presently made the continuation of the tradition of putting out climatological handbooks containing all this information practically impossible. The requirement has arisen to work out

*Numbers in the margin indicate pagination in the foreign text.

and apply new, more economic, and bigger capacity methods for storing this information. And nevertheless everything which is available to us now in climatology from the data of the usual meteorological observations constitutes in all only the essential features of the climatic conditions of the populated parts of continents. Concerning the oceans and the regions which are difficult to reach, their climatic conditions are known only on the basis of the utilization of data from island stations, comparatively few ship stations, and other observations. Such a condition of the climatic statistics seriously restrains the development of physical and dynamical climatology (up to the present time, for example, there is not enough reliable data concerning rainfall over the oceans, since the data of island stations can scarcely be considered to be representative).

The appearance of meteorological satellites has introduced radical changes from the point of view of the possibilities of further development of global and regional climatology [1, 2]. In the first place, for example, success has been achieved in obtaining extensive data on the climatology of our planet's thermal balance on the basis of experiments [3]. The presence of a large number of television and infrared images of cloud cover, which characterize the distribution of cloudiness over the Earth's entire surface at different times, has made it possible to construct objective maps of the global cloud cover.

But at the same time it should be emphasized that only in 1969 were the first steps taken in the direction of utilizing satellites for sounding the atmosphere with the aim of obtaining data about such basic meteorological elements as the temperature and humidity of the air [4, 95]. Concerning the determination of atmospheric pressure, wind velocity, rainfall, and a number of other meteorological elements by means of satellites, the prospects here have still not been defined with sufficient clarity.

Although the first decade of the development of satellite meteorology, which concluded in 1970, has been marked by successes in obtaining data only /4
about the planetary cloud cover and the emergent radiation (in this respect satellite meteorology has developed somewhat one-sidedly), it is possible to

state with complete definiteness that a new direction, which can be called satellite climatology, has arisen in the years past and has been widely developed. The essential content of this section of climatology is presently associated mainly with the investigations of regularities in the planetary distribution of cloud cover and the emergent radiation fields in various regions of the spectra. However, the presence of various and stable connections of the cloudiness and emergent radiation fields with many other meteorological parameters have also made possible the investigation of the temperature fields of the underlying surface (including the oceans) and the lower stratosphere as well as the fields of the geopotential, vertical motions, and many other characteristics. The images of the underlying surface obtained in the absence of clouds have permitted studying regularities in the distribution of snow and ice cover. Recent measurements of the microwave emergent radiation from the Kosmos-243 satellite [5, 6, 93] have revealed definite prospects for obtaining data about the amount of water vapor and liquid water in the atmosphere's interior and for determining the state of the sea's surface, the wind velocity, and so on. It cannot be doubted that in the future satellites will become the main source of information characterizing the distinctive features of our planet's climate in all its variety. Presently, the concept of satellite meteorology has already become familiar. The concept of satellite climatology will occupy just as permanent a place in the meteorological dictionary.

We should emphasize that from the point of view of climatology satellite measurements are valuable not only by virtue of their global nature but also in their unique capability to furnish information about such characteristics (components of the radiation balance of the Earth-atmosphere system, the spatial distribution of cloudiness, and so on) as could be adequately determined only with the help of satellites. The possibility of making direct measurements of average quantities has little value. It is sufficient to recall in connection with this fact that, for example, in the construction of climatic maps on the basis of ground-based data it is necessary to extrapolate arbitrarily the data of individual stations over vast territories. The instruments mounted on a satellite offered the possibility of obtaining

results of measurements which refer to different scales of spatial averaging, from the very small to millions of square kilometers. In the case of determining the vertical temperature profile from data of satellite spectral measurements of the emergent radiation, three-dimensional averaging is carried out: over area (of the order of 10^4 km^2), because of the use of instruments which have a corresponding view angle, and over the vertical, because of the information restriction of the measurement data which permits finding only a smooth temperature profile [4].

Although satellite climatology has only just been conceived, the presence /5
sufficiently vast amount of observational data, whose results have been analyzed in the large number of papers published up to the present time, introduces the necessity of generalizing the accumulated data. It is even more important to carry out this generalization in view of the approximate times for carrying out the Program for the Investigation of Global Atmospheric Processes (PIGAP). There is no doubt that one of the important results of carrying out PIGAP and the subprograms preceding it (experiments -- tropical, Atlantic, polar, energy, and so on) appears to be obtaining meteorological information (both the usual and satellite), which appears to be an important contribution to the subsequent development of climatology.

We turn now to a step-by-step discussion of the results obtained.

1. Cloud Cover

The large volume of data relative to cloud cover which has been obtained with the help of meteorological satellites has permitted first of all working out very detailed classifications of cloudiness observed from space [2, 7]. One of these classifications has been proposed by D. M. Sonechkin [8] on the basis of an analysis of television information obtained with the help of satellites of the Soviet "Meteor" meteorological space system.

Classification of Cloudiness

As D. M. Sonechkin has shown, the texture (structure of the finest details) of an image (the spatial resolving power of the television images of the earth obtained with the help of Soviet meteorological satellites of

the "Meteor" system amounts to about 1 × 1 km) is the most informative factor from the point of view of the essential features of the form and amount of clouds. Therefore, it was precisely the texture which was taken by Sonechkin as the basis of his classification of typical images. The structure of large details was also utilized, but as a secondary indication. This kind of classification indicated the existence of three basic types of television images: dull, granular, and filamentary.

The presence of any nonuniformities in the image's tone is characteristic for the dull texture (see column 5 of Figure 1). As is evident, the television images differ in a specific case only in brightness (the use of seven brightness gradations is, of course, arbitrary). Such images are characteristic of cloudless sections of a water surface, dry lands in regions of sufficient moisture (5 E, F, G), arid sections of dry land (5 D, E), continuous ice or snow cover (5 A, B, C, D), and continuous stratus cloudiness (5 A, B, C). We should emphasize, however, that the brightness of an image is not a discriminating indicator, since the most /8
varied objects can possess practically the identical brightness (for example, clouds and snow).

The granular texture of an image (see columns 1 and 2 of Figure 1) is characterized by the presence of clusters of spots of light or dark tone. The smallest bright spots (grains) usually correspond to cumulus clouds (1 D, E, F, G). Dark grains on a bright background (1 A) indicate, as a rule, the existence of stratocumulus clouds (openings in the clouds stand out as grains). However, cumulus clouds in the zone of the Sun's bright spot can have the appearance of dark spots (1 C). Dark spots correspond not to the clouds themselves but to their shadows. Gaps and thin spots in the sea ice also appear as dark spots (1 B), but they differ in the angularity and sharpness of their outlines. The large bright grains represent thick cumulus clouds (2 B), stratocumulus cloudiness (2 A, C, E), and altocumulus clouds (2 D), and also combinations of these.

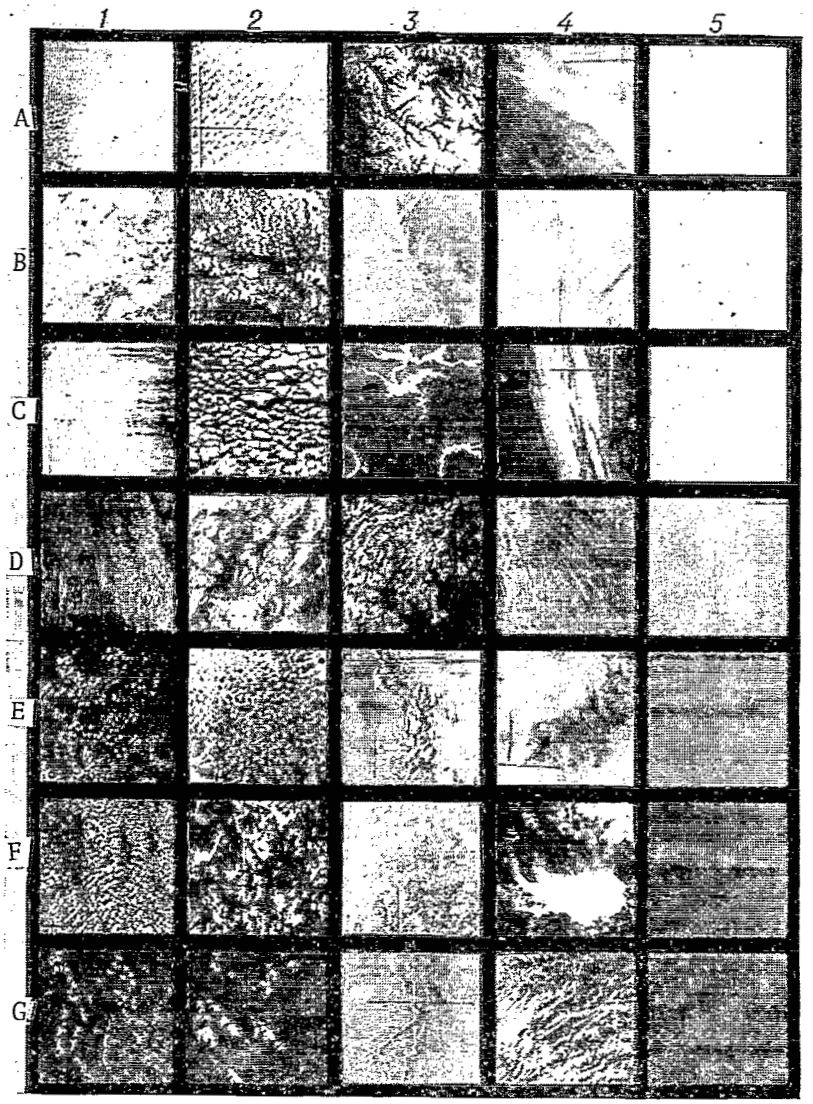

/6

Figure 1. Typical Textures of Television Images of Cloudiness and the Earth's Surface.

/7

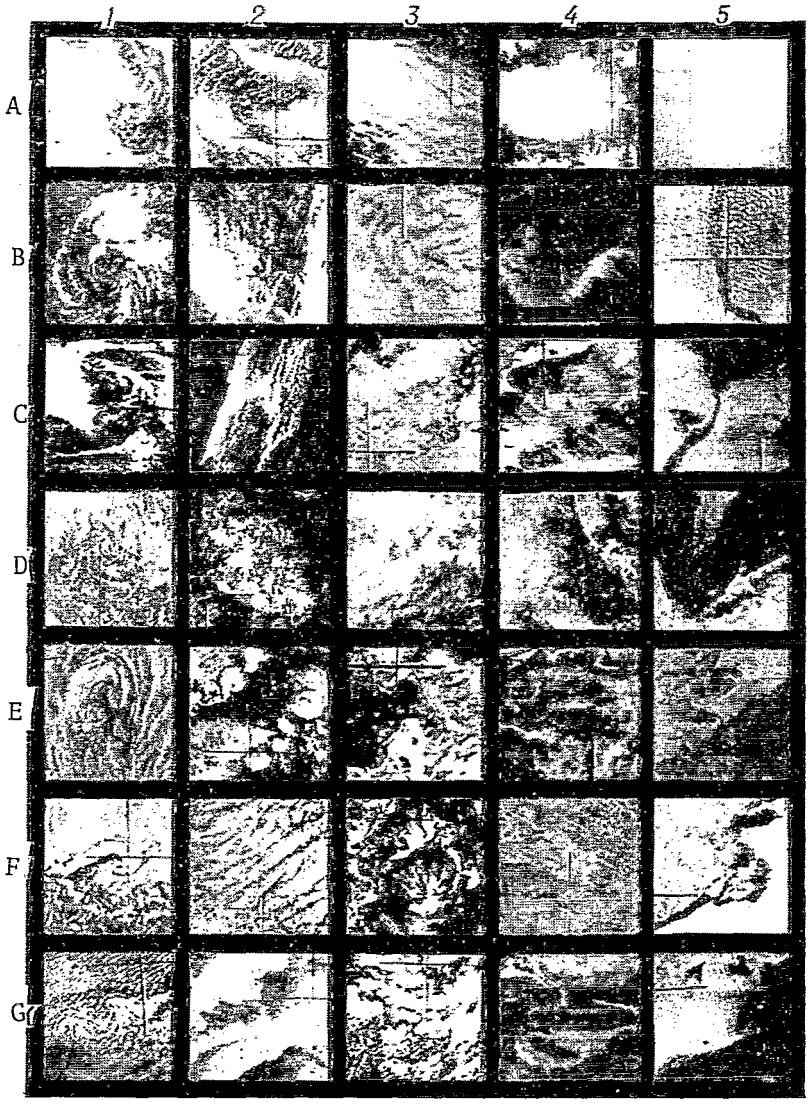

Figure 2. Typical Mesostructures of Television Images of Cloudiness and the Earth's Surface.

The existence of lineaments, filaments, and bands with indistinct edges, which reflect the presence of cloudiness of the intermediate and upper levels, is characteristic for the filamentary texture of an image (see column 4 of Figure 1): for example, compact cirrus against a background of dry land (4 A), stratocumulus clouds (4 C), and so forth. However, sometimes it is possible to observe the Earth's surface (4 D), river valleys), chains of small cumulus clouds (4 G), and so on.

Figure 2 illustrates an example of the classification of large (mesoscale) structures of cloud formations. This very branched classification includes a large number of various objects. One of the most typical categories are cloud vortices (column 1 of Figure 2). Large-scale vortices (1 A, B, C, D) belong most often to occluded extratropical and tropical cyclones. The most frequently observed mesoscale vortices by far arise on the leeward side of islands (1 B, G), near the high coasts of continents (1 E).

In Columns 2-5 of Figure 2 are presented as an example, the images observed most often which do not have geometrically correct mesostructure. Thus, for example, frames 2 A, B, and C represent combinations of cirrus and cumulus cloudiness, but 2 D, E, F, and G correspond to the presence of just cumuliform clouds of the intermediate and lower levels. Images largely of the Earth's surface are reproduced in columns 4 and 5.

The use of classification of television images for the purpose of identifying cloud systems makes it possible to identify more reliably the weather-forming processes from the characteristic peculiarities of the cloudiness structure.

Climatology of Cloudiness and Snow Cover

The large volume of data relative to the planetary distribution of cloud cover which has been obtained with the help of meteorological satellites has permitted beginning in recent years a comparison of world maps of cloudiness for various dates. At the Hydrometeorological Research /9
Center of the USSR such maps have been compared from March 1965 and are

constructed for the northern and southern hemispheres in stereographic projection at a scale of 1:30,000,000 [9]. In addition, maps are also constructed of the cloudiness of the tropical zone (45° N. Lat. -- 45° S. Lat.) in Mercator projection at the same scale. In those cases in which it is possible, the satellite data are supplemented by the results of the observations of ground-based stations. An analysis of the maps of cloud cover has permitted a detailed study of the regularity of the spatial-temporal variability of cloudiness. For example, it has been discovered that although the distribution of clouds over the northern hemisphere is variable both in space and in time, the amount of clouds above the hemisphere as a whole varies comparatively little from day to day and from month to month. During June, July, and August of 1965 variations in the area of the hemisphere covered by clouds did not exceed 10%. The spatial distribution of cloudiness on the average maps is characterized by its clustering in the temperate latitudes and near the Equator. The smallest amount of clouds is observed at tropical and subtropical latitudes [99-102].

Photographs of the Earth from great distances serve as a very obvious means of analyzing the "instantaneous" global fields of cloudiness. V. A. Bugayev and T. P. Popova [78] have completed such an analysis, using a color photograph of the Earth obtained by the Zond-7 space station on August 8, 1969 from a distance of 70,000 km.

In the USA investigations in the area of satellite climatology have begun on the basis of the utilization of nephanalysis maps which initially (up to January 1964) provided for the use of seven gradations in the amount of clouds and later for four gradations. The map of T. F. Clapp [36, 85] and J. C. Sadler [87] was obtained in precisely this manner. Similar original data was used in the recent work of F. A. Godshall, L. D. Allison, E. R. Kreyns and G. Warnecke [82, 86]. These authors prepared an atlas of the average monthly maps of the cloudiness distributions in the tropical zone of the Pacific Ocean for January, April, and August and October during the period from August of 1962 until August of 1968 (data of six satellites of the Tiros series and three satellites of the ESSA series).

Quantities taken from nephanalysis maps are averaged over areas of 2° in latitude by 2° in longitude for a band of latitude from 30° N. Lat. to 25° S. Lat. and for a band of longitude from 100° W. Long. to 130° E. Long. The choice of the months mentioned above was determined by the desire to investigate periods of maximum variability of the large-scale circulation in the region under consideration.

Analysis of the cloud cover distribution maps constructed in [82] indicate the existence of significant variability of the cloudiness conditions from year to year (in the same months) and also in the dependence on the time of year. However, on any map the essential climatological peculiarities are easily identified. This situation is related, for example, to the band of cloudiness between the parallels of 5° and 10° N. Lat., which is associated with the extratropical zone of /10
convergence and the location of the equatorial thermal counterflow.

Satellite television information in the analog form [35, 37, 88] and digital form [11, 84, 91] has also been used for constructing climatological maps of the cloudiness, and sequential photographic exposure of images of cloud cover has been applied [38].

Most recently the construction of diurnal global maps of the cloudiness and maps of the amount of clouds averaged over various time intervals for the equatorial band of latitudes 35° N. Lat. -- 35° S. Lat. (Mercator projection) and for both hemispheres (polar stereographic projection) has /11
been carried out automatically with the help of computers. An example of the planetary cloudiness fields based on observational data in both hemispheres for October 29, 1968 is presented in Figure 3 [10]. The construction of such maps is possible only upon the utilization of the most powerful contemporary computers. In the process of reducing the television data the computer carries out an automatic geographical tie-in of them and the plotting of a grid of geographical coordinance. Along with the daily cloudiness maps the construction of planetary distribution of the cloud cover averaged over various time intervals is also carried out [11]. Simultaneously the brightness values are averaged over areas containing 64 × 64 separate points

(in this case the number of brightness values for each hemisphere is equal to 4,096), which corresponds to the step of the spatial grid applicable in numerical weather predictions. /12

Fifteen gradations of the brightness value are used for presenting the brightness field. Also averaging of the brightness over areas of 8 × 8 separate points have been applied for the purpose of investigating the mesostructure of the cloud cover. Average five-day maps of the cloudiness have been constructed operationally since November 1967. Averaging over more extended time intervals is being carried out in the course of experiments.

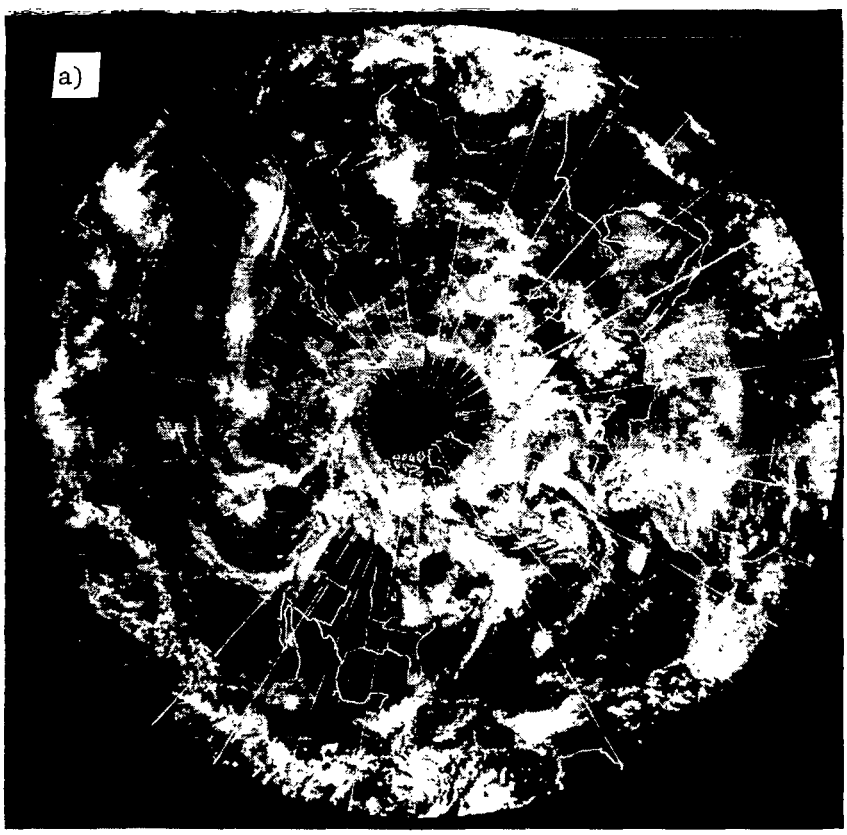

Figure 3. Maps of the Planetary Cloudiness Distribution.
a -- Northern Hemisphere, b -- Southern Hemishpere.

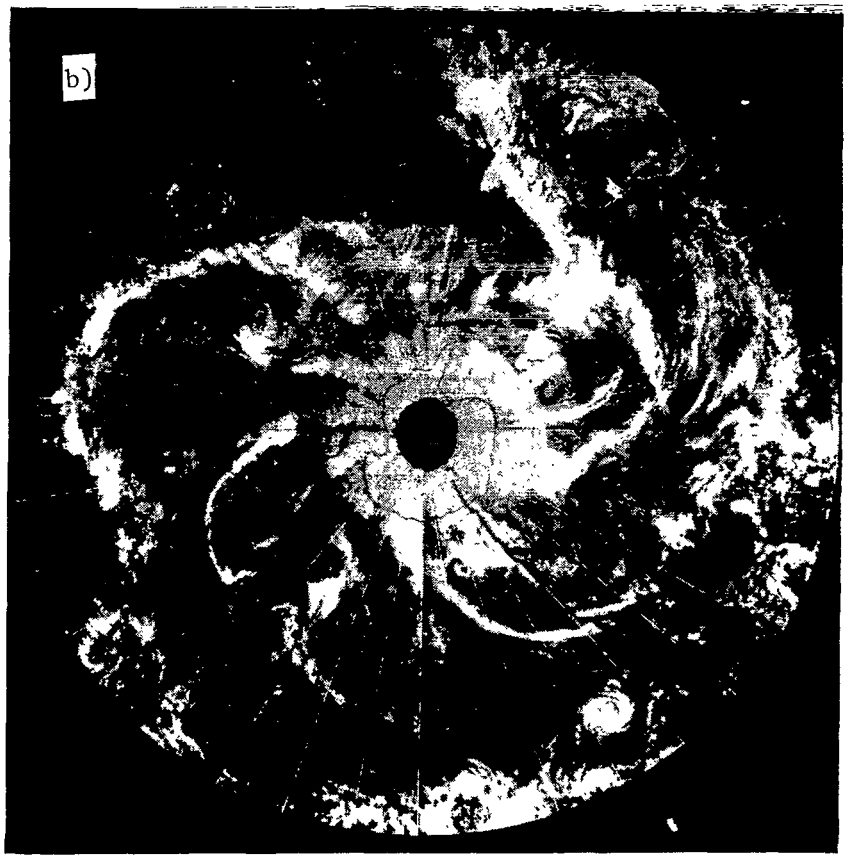

Figure 3. (Continued).

As an illustration an average map of the cloudiness distribution in the northern hemisphere for June-August of 1967 is presented in Figure 4. This map reflects the well-known tendencies towards a decrease in the amount of cloudiness in tropical and subtropical latitudes (we point out that artificial enhancement of the image contrasts is employed in the construction of such maps; if this enhancement were not employed almost the entire hemisphere would be rather bright) Here, for example, the dark belt of the subtropical high pressure maximum stands out distinctly, as does the narrow bright band of the intertropical convergence zone. It is evident that the great brightness of the polar cap and Greenland is produced to a significant extent by the effect of snow cover. /13

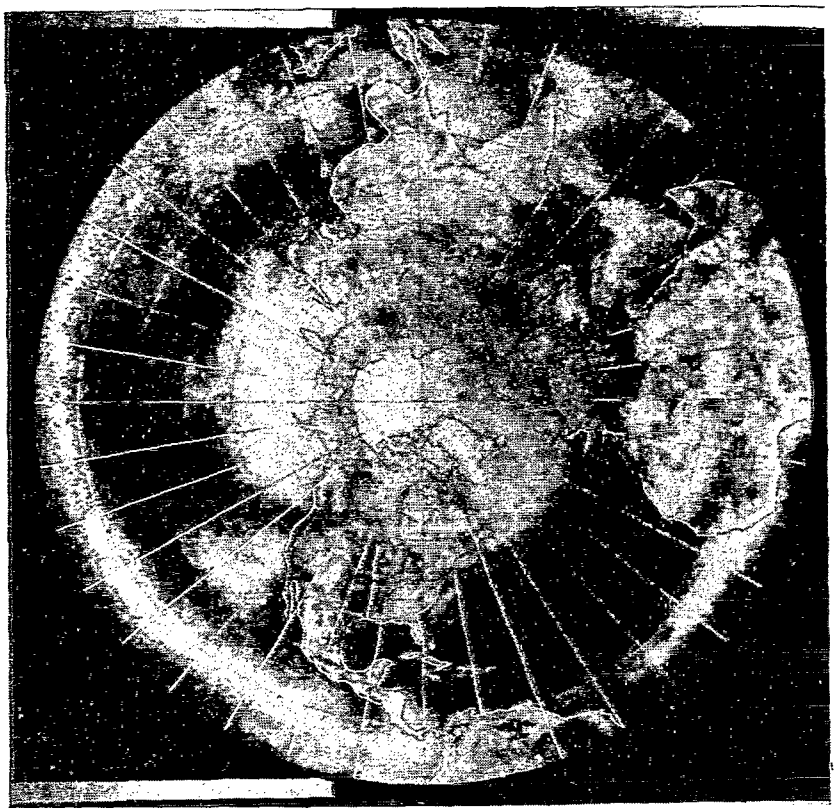

Figure 4. Mean Seasonal Cloudiness Distribution in the Northern Hemisphere (June-August 1967).

It is natural that in the course of averaging the brightness field the effect of unstable cloud systems is smoothed out. Only the individuality of the most stable cloud formations is maintained. The complete elimination of the unstable background by means of constructing brightness fields on the basis of minimum or maximum values is of interest in the solution of a number of problems.

It is easy to understand, for example, that averaging with respect to minimum brightness values leads to the "filtering out" of the cloudiness. An example of the construction of a map of the minimum brightness distribution in the northern hemisphere on the basis of data from the ESSA-9 meteorological satellite for the five-day period April 14-18, 1969 [12-13] is illustrated in

Figure 5. The sharp contrast between the dark and bright zones of the map in the south is caused by the fact that snow or ice cover occurs to the north of the boundary between the zones (it is clear that in the presence of snow or ice the Earth's brightness is always high, independently of the cloudiness conditions; it is natural that television images could not be obtained for the zone of polar night, because this zone is dark). It is evident from this that maps of the minimum brightness are a good method for tracing the boundaries of snow cover or ice. As E. P. McClain and D. R. Baker [12] have shown, the optimum averaging period (taking into account the necessity of "filtration" of the cloudiness and the variability of snow cover or ice conditions) amounts to from three to seven days.

If we average the brightness field only according to its maximum values (see Figure 6, which is borrowed from the reference [11]), the dark regions in such a case will correspond to those regions in which there were no increased brightness values during the entire averaging period (accordingly, no clouds or snow). On the contrary, bright regions reflect the existence of intense cloudiness (or snow and ice). The brightest cloudiness of vertical development is usually accompanied by rainfall. Therefore, bright regions (if these regions are not snow or ice) can be associated in the present case with precipitation zones. One more possibility of interpreting maximum brightness maps consists in their utilization for tracing the trajectory of rapidly-moving stable cloud systems.

One of the main difficulties of utilizing the procedure of simple or selective averaging of the brightness fields consists in the fact that the television instrumentation permits obtaining only a very distorted distribution of the absolute brightness values. Therefore, we should emphasize in this connection the great urgency for the application of scanning photometers for sufficiently correct reproduction of the field of absolute brightness values.

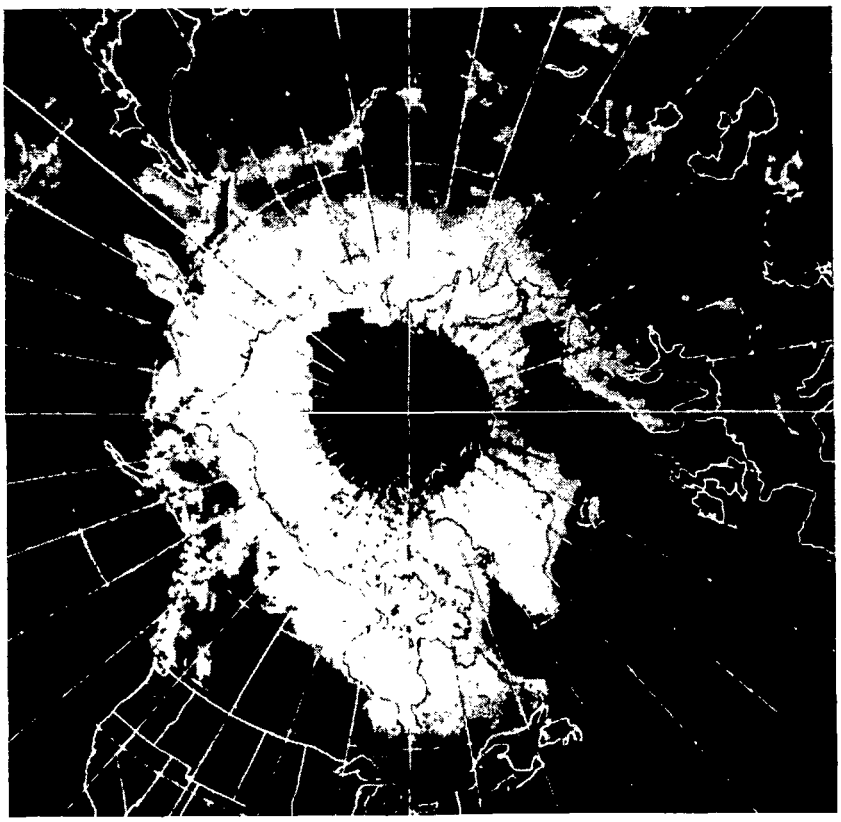

Figure 5. Average Distribution of the Minimum Brightness in the Northern Hemisphere for the Five Days (April 14-18, 1969). Data from ESSA-9.

The attempt to analyze data from geostationary satellites [14, 15, 92, 97] clearly attests to this fact. Photoelectric scanning photometers mounted on the ATS-1 and ATS-3 geostationary satellites permit obtaining not only images of the Earth, consisting of 2,000 lines (ATS-1) or 2,400 lines (ATS-3), but also absolute brightness values. The data records of the photometer readings in digital form contain the brightness values of each of the scan lines, which are located every 1.8 km (the distance between successive lines amounts to 3.6 km and corresponds to the value of the photometer's spatial resolving power) along the corresponding circle of latitude. The photometer readings are linear functions of the brightness to a large extent over a wide range of brightnesses. Therefore, the determination of relative brightness values can be /15 carried out simply and reliably.

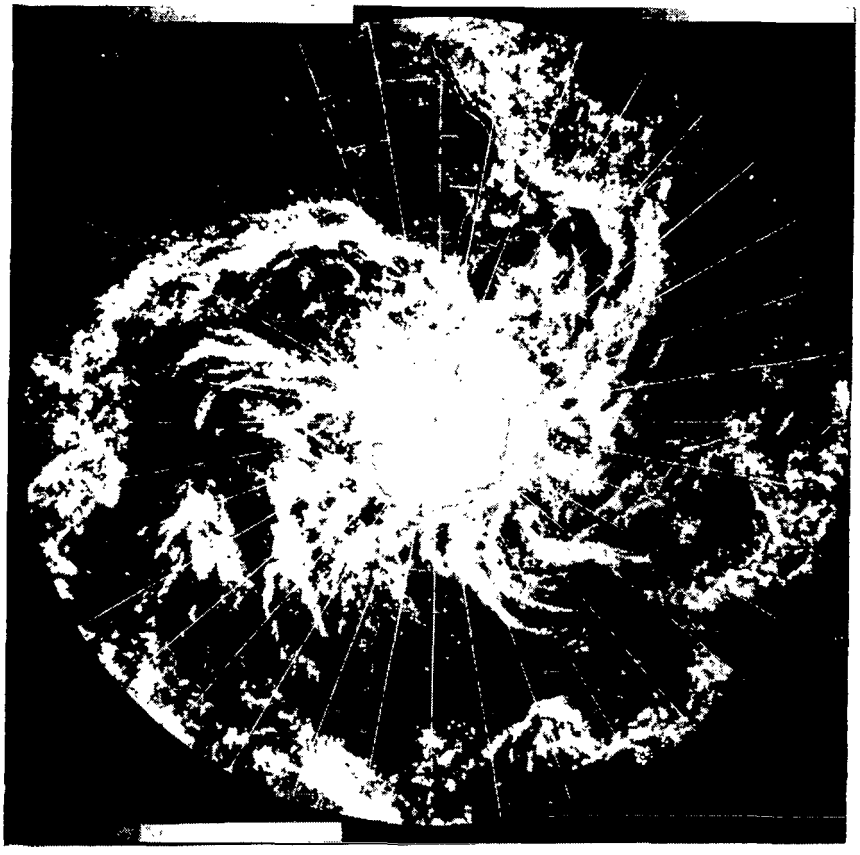

Figure 6. Average Distribution of Maximum Brightness in the Southern Hemisphere for the Five Days (December 7-11, 1967). Data is from ESSA-3.

T. H. Vonder Haar [14], for example, has discussed the relative brightness fields in a region of a frontal cloudiness zone. Such maps of the brightness fields make it possible to localize exactly regions of maximum brightness, which correspond to the locations of the occurrence of intense precipitation. Similar small-scale maps, which refer to extended areas at various times, are a good method for tracing the dynamics of cloud cover, and also for studying air currents. Data which refers to the region of solar bright spots over the ocean contains information which permits one to characterize roughness and wind velocity.

The emergent radiation field in the region of the atmosphere's transparency /16 window at 8-12 microns [96] is, similarly to the brightness field in the

visible spectral region, a sufficiently reliable indicator of the planetary distribution of cloud systems. Data concerning the emergent radiation field in this transparency window has been widely utilized earlier within the framework of "radiation" synoptics (see the references [2, 4]). The recent work of L. J. Allison et al., [81] contains an attempt to utilize the Tiros VII data in the form of quasi-global monthly maps of the radiation temperatures (for the transparency window at 8-12 microns) for analyzing the peculiarities of the atmosphere's general circulation. This attempt has continued the earlier investigations undertaken in this direction [37, 88, 89]. This attempt turned out to be completely successful, since the authors [81] were able to trace in sufficient detail the peculiarities and seasonal variability of the general circulation on the basis of the use of radiation temperature maps (in spite of the sketchiness caused by a whole series of reasons: averaging without taking account of the daily run of the radiation temperature, the absence of the possibility of completely reliable discrimination of clouds and the underlying surface, and so on).

One of the most reliably identifiable peculiarities of the atmosphere's total circulation is the intertropical convergence zone (ICZ).

The quasi-stationarity of the ICZ for periods of the order of several months permits an analysis of local peculiarities of the tropical circulation which is especially important for water areas of the oceans. But, for example, during the course of almost an entire year a band of cloudiness has been observed over the Pacific Ocean which has stretched from Easter Island northwest in the direction towards the Equator and is associated with a high pressure ridge in the upper troposphere. This cloudiness zone is usually "blended" with the ICZ between Caton Island and New Guinea. The ridge mentioned encroaches on the subtropical belt of increased pressure and is the connecting link between the circulation of the tropics and the extratropical latitudes.

The papers of I. V. Bugayeva and L. A. Ryazanova [79, 90] have a very important significance for determining the possibilities of using maps of the radiation temperature for the 8-12 micron transparency window for the purpose

of analyzing cloudiness conditions and distinctive features of the atmosphere's general circulation. These papers are devoted to a demonstration of the effect of various types of cloudiness on the values and structure of the radiation temperature fields on the basis of data from the Kosmos-144 and Kosmos-184 satellites. The television and radiation data of these satellites were used to construct monthly maps of the cloudiness for April and July and the radiation temperature for January, April, July, and October of 1967. A comparison of these maps revealed a clear picture of their qualitative agreement. Therefore, I. V. Bugayeva and L. A. Ryazanova have detected, just as clearly as the authors of the reference [81], the ICZ as a characteristic peculiarity in the form of a band of lowered values of the radiation temperature which stretches along the Equator. The zone of summer monsoon circulation, /17 which is extended along the eastern coast of Asia, is reliably identified as a cold trough.

2. Wind, Vertical Motions, and Precipitation

The close connections between cloudiness fields and atmospheric motions permits, on the basis of empirical data, posing the problem of determining the wind and vertical motions from the cloudiness field and its variability.

Therefore, the data of meteorological satellites now introduces an important contribution to the investigation of atmospheric circulation in the tropics. Thus, for example, television images of the Earth have permitted investigating the effect of the motions of various scales on the formation, development, and spatial structure of clouds and tracing all phases of evolution of tropical cyclones. Observations behind the clouds make it possible to obtain information about peculiarities of air currents.

The following are among the most important manifestations of the atmosphere's general circulation which are amendable to investigation by the use of satellite television information: 1) subtropical jet streams at the northern boundary of the general circulation's tropical zone which were discovered from the characteristic bands of cirrus cloudiness; 2) air currents in the upper troposphere which intersect the Equator (the satellite data have shown that this phenomenon is by far more typical than it was assumed earlier);

3) air exchange between low and high latitudes (sometimes moist tropical air, invading the north, reaches 50° N. Lat.); 4) bands of equatorial or intertropical convective cloudiness which are enormous in extent (the most stable during the entire year is a band situated over the Pacific Ocean in the 5-10° N. Lat. zone; significant seasonal migration is characteristic for similar bands over the Atlantic Ocean); and 5) tropical storms (it has been repeatedly verified, for example, that many Atlantic storms arise in Central Africa; it has been discovered that usually the center of circulation of a developed storm is located beside but not under the main cloudiness system of the storm).

Geostationary satellites have turned out to be an exceptionally effective method for tracing the development for various synoptic features. Thus, for example, it was possible to trace with the help of the ATS-1 satellite the evolution of the typhoon Sara in the course of its migration across the Pacific Ocean (135° W. Long. -- 150° E. Long.) from the stage of its generation in September of 1967 southeast of the Hawaiian Islands until its destruction two weeks after this (west of Vancouver Island).

Images of the Earth obtained with the help of the ATS-1 and ATS-3 geosynchronous satellites first permitted the study of the dynamics of cloud cover in the region of the tropics, which has important meaning for understanding the weather-forming processes which arise here. Investigations of the cloud bands of the intertropical convergence zones (ICZ) have attracted especially /18 great attention. An analysis of the individual images has shown that the cloudiness of the ICZ is a combination of large nephsystems in the form of bands with thicknesses from 5° to 10° of latitude. The average distance between these systems varies from 10° to 30° in longitude, i.e., close to the value for a wavelength (2,000 km) of the easterly waves in the tropics, whose development is accompanied by a widening of the ICZ and frequently results in the initiation of tropical storms. The large nephsystems mentioned have received the designation of cloud accumulations.

T. Fujita et al., [16] have constructed motion fields for clouds over several days on the basis of the observational data (images of the cloud cover) from the ATS-1 satellite during September of 1967 for the eastern part of the

tropical belt of the Pacific Ocean. The procedure for determining the drift velocity of the lower-level clouds, whose dimensions do not exceed 25 km, is based on using five consecutive images obtained with an interval of 20 minutes. The progress of data on the drift velocities of clouds has permitted constructing fields of flow lines (taking into account possible extrapolation) with the locations of cyclones, anticyclones, and troughs plotted on them. A comparison of the drift velocities with data on the wind at the Earth's surface based on observations on ships and islands has shown that the cloudiness band of the ICZ consists of several cloud accumulations, which are associated with disturbances in the pressure field near the Earth's surface.

Calculations based on data for the field of flow lines of the divergence fields and with respect to the vorticity, and also the construction of maps of the isotachs (isolines of the wind velocity), have revealed that the zone of maximum convergence is located southeast of the cloud accumulations, and the regions of maximum vorticity coincide with the centers of cyclonic circulation. However, in the case of a tropical storm the locations of the convergence and vorticity maxima coincide. Thus the air currents which accompany the accumulations are significantly different from those which are characteristic for storms. Therefore, the cloud belts of the ICZ are characterized to a far greater extent by "vorticity" than by "convergence", and thus it would be more correct to speak of an intertropical vorticity zone.

Estimates of the effect of the various factors which determine the dissipation of vorticity by means of the use of data on the divergence and vorticity fields have shown that the dissipation conditions are closely linked with the temperature of the ocean's surface, whose influence can result in a decrease in the interaction between the atmosphere's lower layers and the underlying surface in the boundary friction layer. An important peculiarity of the eastern part of the Pacific Ocean's tropical zone is the formation here of anticyclones as the result of the intrusion across the Equator of air currents from the southern hemisphere. An analysis of the trajectories of such air currents under various conditions has shown in particular that the /19
deepest intrusion into the northern hemisphere (to a latitude of about 20° N. Lat.) occurs in that case in which the angle at which the Equator is

intersected is equal to 170°. In the case of an angle less than 90°, the trajectories do not reach latitudes higher than 8° N. Lat.

Thus the possibility of an almost continuous tracking of the dynamics of the cloud cover from geosynchronous satellites has turned out to be very fruitful from the point of view of obtaining data on air currents.

As L. A. Anekeyeva [17] has shown, approximate estimates of the direction and wind velocity (in the presence of cloudiness of vortex structure) can be made on the basis of data from quasi-polar meteorological satellites. Observational data from March 1966 through March 1967 over the territory of the Soviet Union, Western Europe, and the northeastern Atlantic (412 cloud vortices were investigated in all) served as the original data. The form of a cloud vortex is modeled after a hyperbolic spiral.

Then histograms were constructed for 40 parts of the vortex which showed the distribution of the angle between the directions of the cloud band and the wind (wind data for each station located in the vortex region were taken for the standard isobaric surfaces -- from the Earth's surface to the 300 mbar level). It turned out that the distribution law of the inclination angle is close to the normal distribution law. This fact has permitted constructing a table of the most probable values of the inclination angle for various sections of a vortex, with the help of which it is possible to determine the wind direction at any point of a region occupied by vortex cloudiness. Inspection of this table shows that under the conditions of a free the wind is inclined most often to the left of the cloud band, and the value of the inclination is 20°. At the Earth's surface the opposite situation is observed. Data on the most probable values of the wind velocity at various levels can be obtained by means of a statistical reduction of the observational results (also see [18]). Spots of specular reflection on the surface of the sea can serve as a good wind indicator [94].

E. C. Barret [22] has proposed a procedure for estimating the monthly precipitation totals on the basis of utilizing nephanalysis maps constructed on the basis of satellite television images of the cloud cover. With the help of the nephanalysis maps the following initial parameters are determined:

1) the average monthly amount of precipitation in % (four gradations of this parameter are used on the maps: 10, 35, 65, 90%); 2) probability of rainfall and the intensity of precipitation from clouds of the type under consideration (in particular, cumulus, cumulonimbus, stratocumulus, stratus, and cirrus clouds are distinguished on the nephanalysis maps). The probabilities of rainfall and intensities of precipitation assigned to clouds of the indicated types are set on the basis of *a priori* statistics.

A "precipitation coefficient" is calculated on the basis of data on the parameters mentioned above. The effect of orography and elevations above sea level is not taken into account. If clouds of different types are observed /20 simultaneously, notice is taken only of the clouds with the largest precipitation probability. In the absence of such cloud systems accompanied by precipitation, such as frontal zones, vortices, and so on, the parameters for stratus and cumulonimbus clouds are taken with a weight equal to four. On the basis of 29 Australian stations for March, April, and May of 1966 the following correlation link was found between the precipitation coefficient x and the monthly precipitation total y ($y = 0.00200x^3 - 0.05108x^2 + 1.30107x - 0.32750$). This relation was used to construct a map of the distribution of precipitation for July of 1956 for the 90-180° E. Long., 15° N. Lat. -- 30° S. Lat. zone with averaging over areas of 5° in latitude by 5° in longitude. A check of this map against the data for the same 29 stations for July showed that the values referring to 17 stations were completely correct. Evidently, the best results can be obtained when orographical and latitude effects are taken into account.

Ch. S. Novak [19] made an interesting attempt to use the data on the brightness field of systems of cumulus clouds for the solution of the problem of automatic identification of such cloudiness (on the basis of its very great brightness) and also to calculate the direction and velocity of the wind in the upper troposphere (on the basis of the direction of "blowing" and the length of the band of cirrus cloudiness located near the top of the cumulus clouds). As has already been noted above, estimates of the wind velocity also can be carried out by determining the drift velocity of the clouds (consecutive images obtained with the help of geostationary satellites are particularly

suitable for this purpose) and utilizing the empirical dependence of the maximum wind velocity in a hurricane on the dimensions of the central core of the hurricane's cloud systems [2].

Data on the amount of cloudiness can be obtained with far greater reliability than the absolute brightnesses. Therefore, for this reason various attempts have been undertaken to interpret such data on the basis of the utilization of empirical correlation links between the fields of cloudiness and other meteorological elements. S. A. Musayelyan and his co-workers [20,21] have worked out this approach most successfully. In particular, they solved the problem of determining the field of vertical motions from the cloudiness field.

The examples discussed above permit us to draw the conclusion that the results already obtained indicate the outlook for the interpretation of television images of cloud cover with the goal of determining the fields of various meteorological elements from the cloudiness field. Of course, one should bear in mind the fact that the topic of discussion is, in any case, only about the use of empirical correlation links and comparatively crude estimates. The accuracy of such estimates can be significantly increased by the use of scanning photometers to obtain the images. It cannot be doubted that an increase in the accuracy of the procedures of quantitative interpretation of images of cloud cover permits a wider use of these /21
procedures for climatic investigations. In connection with this we note that the interpretation of infrared images of the Earth, whose important characteristic is the possibility of simultaneously having available data about the field of absolute brightnesses of the radiation temperature, opens up various possibilities of this kind.

The possibilities of utilizing infrared images and data on the field of the outgoing emission of the radiation temperature in various spectral regions for determining the temperature and the field of the height of the cloud cover's upper boundary, the field of some characteristics of the atmosphere's energetics, the precipitation field, the field of vertical motions, the geopotential field, the field of other meteorological parameters have been discussed in detail in the monograph [4].

3. Temperature of the Stratosphere

One of the most interesting (and most significant in practice) examples of interpreting data on the emergent radiation fields is the determination of the stratosphere's temperature on the basis of measurements of the emergent radiation in the central part of the 15 micron band of carbon dioxide gas. We will not dwell on a description of the interpretation procedure, which is expounded in detail in the monograph [4]. We will discuss only some results obtained by G. Warnecke [23, 24] on the basis of using the most correct procedure for interpreting actinometric information from the Nimbus II satellite (taking into account the effect of cloudiness) and representing the first example of global data on the stratosphere temperature field.

/22

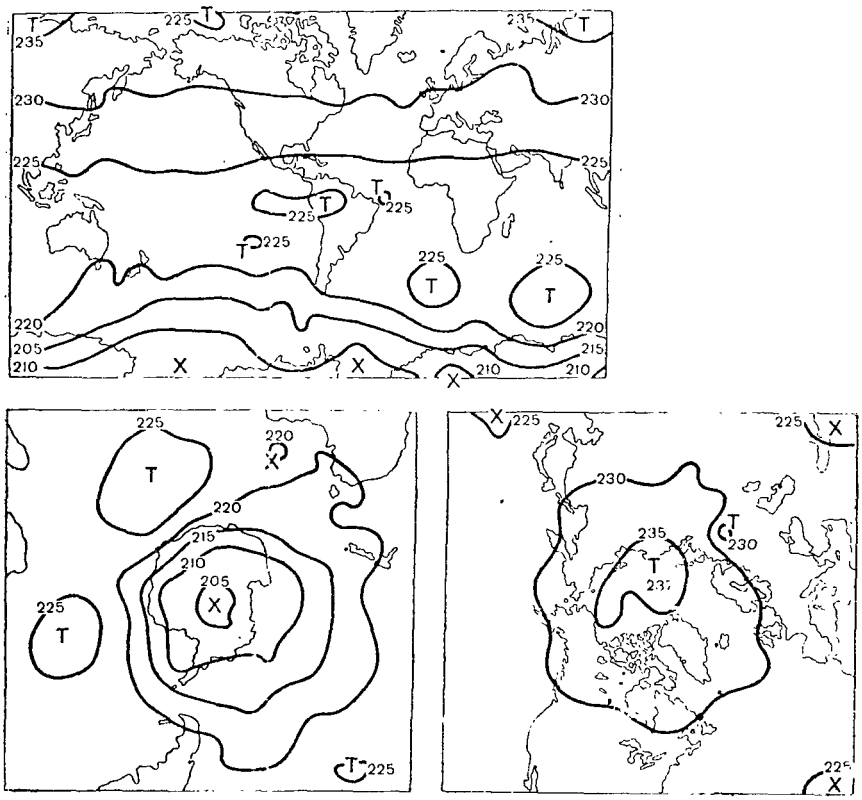

Figure 7. Global Distribution of the Stratosphere's Temperature on May 21, 1966.

Maps of the geographical distribution of the stratosphere's temperature are presented in Figures 7-8 on the basis of data for May 21 and July 24 of 1966 (in the construction of such maps data on the emergent radiation during 24 hours are used). During the period under consideration (the end of May-July) the temperature field in the northern hemisphere was comparatively steady. Thus, for example, clouds of the highest temperatures were located continuously over the norther Arctic Ocean. The horizontal temperature gradients over /23
the entire hemisphere were small. The maximum temperature (240°K) was observed over the North Pole about July 1, 1966. The stratosphere's temperature in the tropics (30° S. Lat. -- 30° N. Lat.) was 220-225°K and increased weakly from the south to the north.

The most dynamic temperature field was observed in the stratosphere in the southern hemisphere. As is evident from Figure 7, already on May 21 a polar vortex, which was maintained during the entire period under consideration, was located over the South Pole. Throughout the time of the first six weeks of this period the temperature field possessed a characteristic asymmetry. Thus, for example, on May 21, 1966 an extensive region of relatively warmer air was extended in the direction of the southern peripheries of the Atlantic and Indian Oceans, which produced a strong meridional temperature gradient. During the next three weeks a shift of the heat centers to the east was observed, as a result of which on June 10 warm air reached Australia and the western sector of the northern periphery of the Pacific Ocean. /24
However, in the second half of June the warm air receded into a zone of low latitudes, and the polar vortex became more symmetric thermally. A similar situation was maintained until the end of July (see Figure 8). A gradual cooling occurred at the center of the vortex from the middle of May (about 205°K) until the beginning of July (196°K), after which the temperature decrease ceased. The maximum cooling was observed, however not in the zone of polar night over the Antarctic, but in regions of the southern periphery of the Atlantic and Indian Oceans (55-65° S. Lat., see Figure 9). A detailed analysis of the variations in the temperature field showed that the distinctive features of the geographical distributions of the cooling pointed out are caused by a temperature wave, which migrates around

the South Pole above the upper part of the temperature latitude zone and which possesses an amplitude decreasing with time (practically to zero in July). This fact indicates the important role of dynamic hypotheses as a factor in winter cooling in the region of the polar vortex of the southern hemisphere.

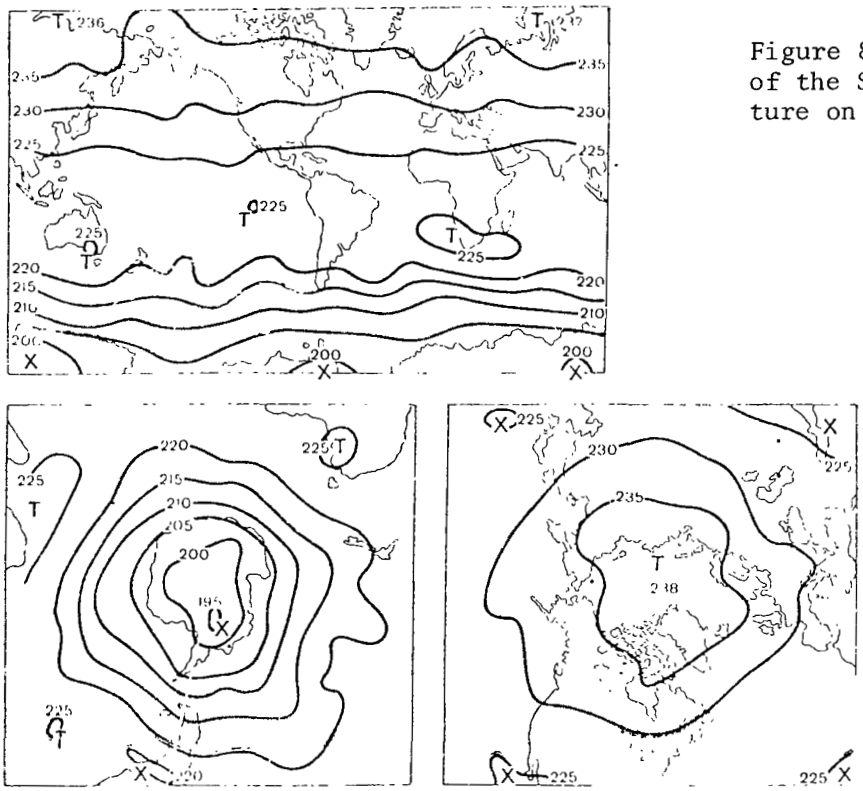

Figure 8. Global Distribution of the Stratosphere's Temperature on July 24, 1966.

The examples discussed above are only an illustration of those possibilities which the use of satellite data opens up for investigations of the stratosphere's temperature field. The rich observational data from the Tiros VII satellite from June of 1963 to July of 1964 in the form of maps of the planetary distribution of average stratosphere temperature values for ten days is contained in an atlas compiled by D. S. Kennedy [25]. There can be no doubt that the subsequent application of the procedure described in the present section will turn out to be a very fruitful one from the point of view of investigations of large-scale processes in the stratosphere.

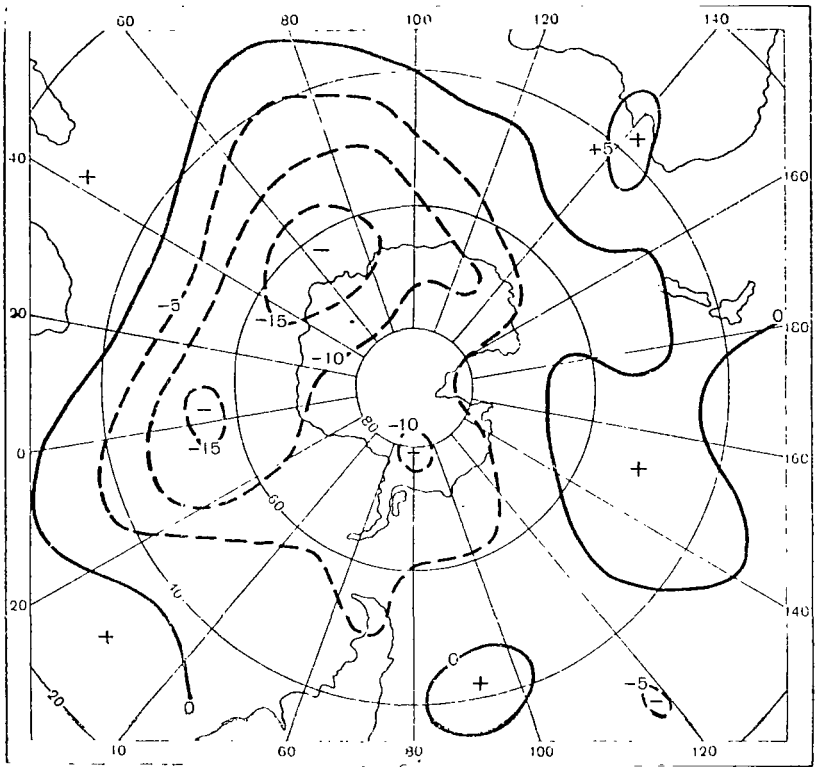

Figure 9. Variation of the Stratosphere's Temperature from May 21 - July 24, 1966.

4. Thermal Inhomogeneities of the Underlying Surface

The infrared images obtained in the absence of cloud cover offer the possibility of studying the temperature field of the underlying surface.

Setting aside the problems of the procedure for determining the temperature from such data (see, for example, the references [4, 26, 27]), we will discuss some examples which illustrate the possibilities of interpreting infrared images of the underlying surface.

An infrared image of the Atlantic sector of the polar cap of the South Pole taken from the Nimbus I satellite on August 29, 1964 is presented in Figure 10. An analysis of this image carried out by W. Nordberg [28] has shown that the temperature of the inner part of the Antarctic ice cap is 210-215°K. Such low values of the temperature were recorded during the entire

operational period of the satellite (from the end of August to the end of September in 1964). Near the edge of the Antarctic continent the temperature increases noticeably, reaching approximately 240°K. The edge of the continent is sharply outlined, due to the presence of a strip of open water, whose width in places reaches 100 km. The maximum temperature in this region reaches 256°K /25 (such a value for the temperature indicates the fact that not only water but also ice must fall into the radiometer's field of view). The higher temperature of the ice cover in the zone of the Weddell Sea and the Atlantic Ocean, which reaches 244°K, permits distinguishing this zone from the continent. Breaks of the sea ice are distinguished as narrow lines of increased temperature. The ice shelf extends to a latitude of about 57° S. Lat., where its borders are on a strip of open water having a temperature of approximately 275°K.

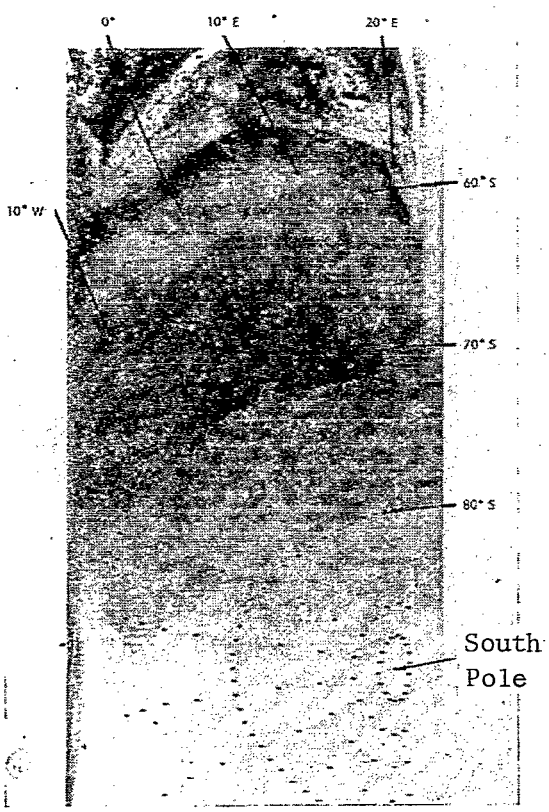

Figure 10. Infrared Image (3.5--4.1) Micron Region of the Spectrum) of the Atlantic Sector of the Antarctic. Obtained from Nimbus I about Midnight (Local Time) on August 29, 1964.

The analysis carried out [29] of infrared images, and also of quantitative data on the radiation field obtained with the help of a scanning radiometer of high angular resolving power mounted on the Nimbus II meteorological satellite, has demonstrated the possibility of utilizing them for tracing the spatial distribution of ice fields. In the discussion of data referring to the water area located between Canada and Greenland, the dark (warm) sections of the images were interpreted as open water, while zones of gray tones (cold) were identified as ice. /26

The authors of [29] showed by comparison with air reconnaissance data that the nighttime infrared images permit reliable tracing of the distribution of ice, especially its large-scale features. The boundaries of the ice-water vision are fixed far more reliably than the inhomogeneity of the ice cover itself (fresh and pack ice, and so on). If the temperature contrasts between ice and water are large enough, it is possible to detect details having dimensions smaller than 8 km.

Although the presence of cloudiness hinders the use of infrared images for analyzing the ice environment, the actual repeatability of the observations is sufficient to obtain very useful data. It is natural, however, that in the wintertime (in the presence of inversion) the problem of distinguishing the ice cover and lower-level clouds becomes difficult, especially for the reason that low continuous cloudiness and fresh ice cover can have a similar structure on the infrared images. The solution of this problem can be lightened by increasing the spatial resolving power of the infrared instrumentation.

Since diurnal infrared images in the spectral region under consideration (3.4-4.2 microns) cannot serve as a method of distinguishing thermal inhomogeneities, they were analyzed together with the data of emergent radiation measurements with the help of a five-channel radiometer for the 0.2-4.0 and the 10-12 micron channels. The combination of all this data permitted, as a rule, reliably distinguishing sea ice from clouds having as high an albedo but a lower temperature (this case is the most difficult in the analysis of television images). The advantage of such data in comparison with the use of

television information consists also in the possibility of applying a mechanical procedure of automatic analysis of multispectral data.

From the point of view of the difficulty of interpreting the infrared images in the presence of small (or negative) temperature contrasts between the clouds and the underlying surface, an analysis of an image of the territory of Greenland obtained from the Nimbus I satellite on September 16, 1964 (Figure 11) is of interest. In the case under consideration the clouds were approximately 20° warmer than the snow-covered underlying surface, whose temperature was about 230°K. Therefore, the cloud bands appear dark against the background of the bright (cold) underlying surface (upper half of the photograph). The lower half of the image is filled by an extensive cloud mass /27 separated from dry land by a very dark strip which corresponds to open water with a surface temperature higher than 280°K.

Figure 11. Infrared Image (3.5-4.1 Microns Spectral Region) of the Territory of Greenland. Taken by Nimbus I near Midnight on September 16, 1964.

The possibility of utilizing infrared images to investigate the temperature field of the surface of seas and oceans has especially important meaning. This fact made it possible first not only to construct sufficiently reliable

climatological maps of the surface temperature but also to investigate its variability [30].

The data on the variability of the ocean's surface temperature (histogram) and the temperature field of the ocean's surface in the region of the Gulf Stream current (Nimbus II) obtained by P. K. Rao et al., [30] are presented in Figure 12. The histograms are plotted on the basis of data for areas 1° in latitude by 1° in longitude. Analysis of the histograms has shown that they are single-peaked in the presence of clouds or continuous cloudiness, while in the case of partial cloudiness they are double- or multi-peaked (á correlation of the main maximum with the temperature of the ocean's surface occurs). The values of the surface temperature are taken as the maximum values for areas of /30 0.5° in latitude by 0.5° in longitude.

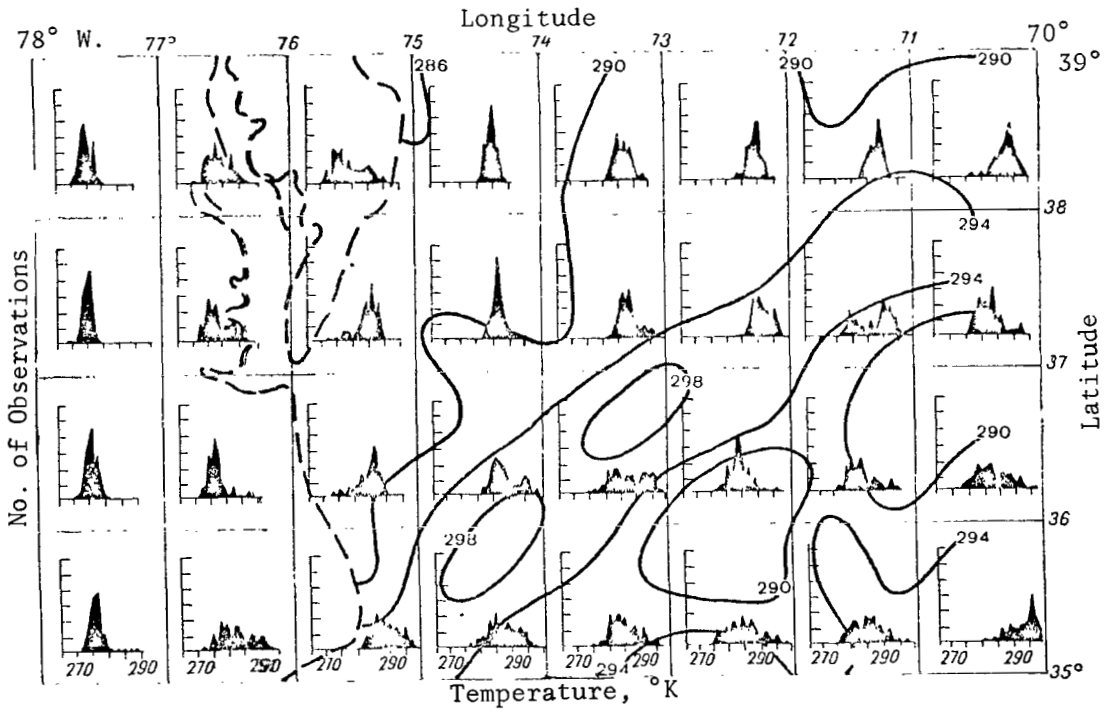

Figure 12. Field of the Average Temperature of the Ocean's Surface and Histograms of the Temperature at Various Points Based on the Nimbus II Data for November 15, 1966.
The dashed curves indicate the position of the coastline

/29

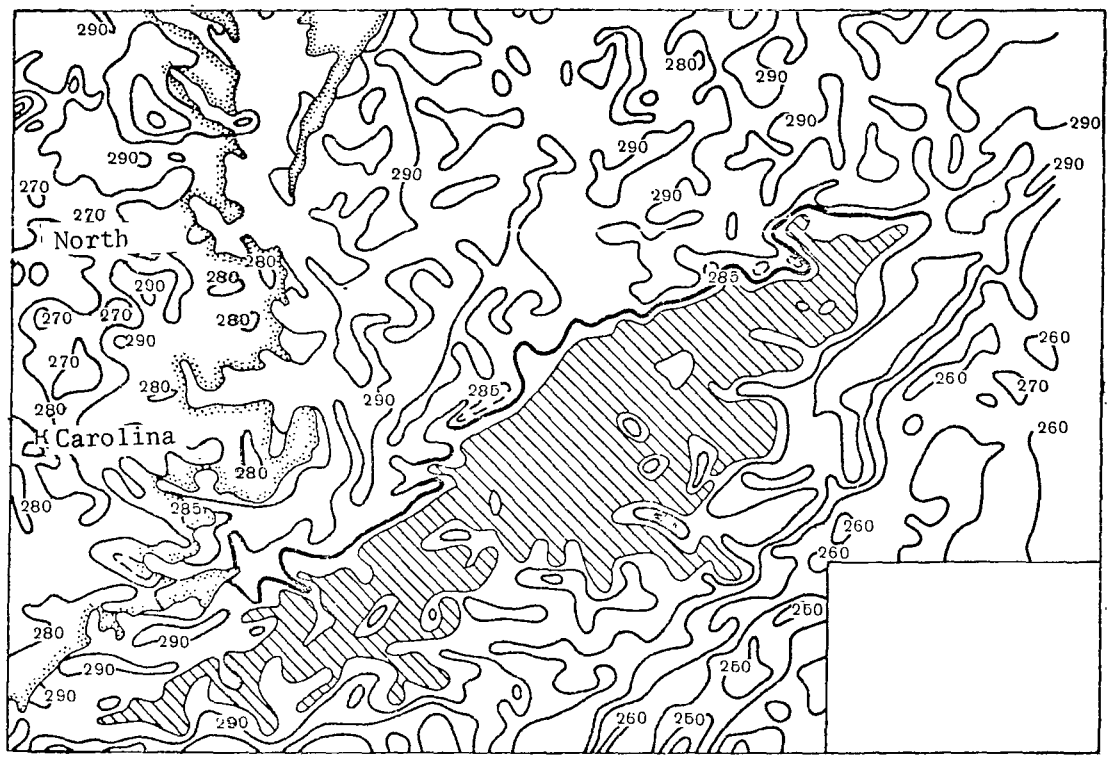

Figure 13. Infrared Image of the Water Area of the Atlantic Ocean in the Region of the Gulf Stream Flow Represented in the Form of Isolines of the Ocean's Surface Temperature. Obtained by Nimbus II on June 2, 1966.

Since the very sensitive infrared instrumentation permits recording small temperature contrasts, an infrared photograph can be used to detect and trace sea currents. The authors of [31] have carried out calculations which have demonstrated the theoretical possibility of solving such a problem. An analysis of the infrared images obtained with the help of the Nimbus II satellite has confirmed these conclusions [32, 33]. The field of temperature isolines of the Atlantic Ocean's surface in the region of the Gulf Stream current obtained on the basis of the utilization of an infrared image for the water area under consideration obtained June 2, 1966 (Nimbus II) is illustrated in Figure 13. The Gulf Stream is clearly distinguished as a zone of increased temperature values. The northern boundary of the flow is outlined very contrastingly.

5. The Earth's Thermal Balance

Besides the television infrared information, the results of satellites actinometric measurements are the most numerous. The topic of discussion in the present case is now not only about the theoretical possibilities or individual illustrations but about the sufficiently settled trend of satellite radiation climatology. Prior to moving on to a discussion of the nature of the problems, we recall that the equation of the thermal (radiation) balance of the Earth-atmosphere system R_s has the form

$$R_s = Q_0(1 - A_s) - F_\infty, \qquad (1)$$

where Q_0 is the rate of arrival of solar radiation outside the atmosphere's boundary, which varies of a function of the distance between the Earth and the Sun; A_s is the albedo; and F_∞ is the emergent long-wavelength radiation.

Procedure for Interpreting the Data of Emergent Radiation Measurements

An attempt to interpret the data of emergent radiation measurements for the purpose of utilizing the regularities of the spatial-temporal variability of the thermal (radiation) balance of the planet has confirmed the advisability of two types of instrumentation: narrow-angle scanning and wide-angle radiometers [1, 4]. Both narrow-angle and wide-angle instruments are mounted on Soviet meteorological satellites [4]. The main advantage of measurements with the help of narrow-angle radiometers is the possibility of obtaining a very detailed spatial distribution of the measurable components of the Earth-atmosphere system's radiation balance. The serious difficulty of interpreting the readings of the narrow-angle detector for the purpose of determining the hemispherical emergent radiation fluxes consists in the /31
necessity of *a priori* specifying the angular distribution of intensity of emergent radiation. The advantage of the wide-angle detector consists in the wide coverage of territory (this simultaneously indicates, of course, that the spatial resolving power is low). Due to the fact that the wide-angle radiometers were mounted on a large number of satellites and have operated a long time, the observational data have accumulated up to the present time for approximately five years [42-44].

In recent years problems of the procedure for interpreting the data of emergent radiation measurements have been discussed very extensively (see, for example, [39, 42, 45]). Therefore, we will restrict ourselves to only short commentaries referring to the most significant aspects of interpretation.

As the authors of [45] have noted, the reduction procedure for the data of actinometric measurements, which can be carried out with the help of meteorological satellites, includes the following steps.

1. The transition from electrical quantities at the output of the radiometer or telemetric system to values of the intensities or fluxes of the radiation at the satellite's altitude (using the results of a preliminary calibration of the instrument and the data of the onboard calibrations).

2. Taking account of the selectivity of the detectors of emergent radiation and also as a discrepancy of the energy distribution in the spectra of the standard source used to calibrate the instrument and the planet's emergent radiation.

3. Taking account of variation of the sensitivity of the radiometers during the operational period and also in the launch phase (as is well known, the uncontrollable variability of the sensitivity of the five-channel radiometers mounted on the Tiros satellites has greatly complicated and prolonged in time the process of interpreting the results of the measurements).

4. Conversion of the intensities or fluxes of the emergent radiation at the satellite's level into hemispherical fluxes for values of the albedo (for measurements in the short-wavelength region of the spectrum) for the conditions of the atmosphere's upper boundary.

5. The first three problems are solved on the basis of utilizing the data of pre-flight and onboard calibrations. Leaving aside the very Earth important problem of the calibrations, we will turn to a discussion of the source of the problems enumerated above.

The difficulty of solving this problem is distinguished by the fact that it is necessary to determine the radiation flux F, i.e., to carry out the integration on a hemisphere as

$$F = \int_0^{2\pi} \int_0^{\frac{\pi}{2}} J(0,\ \beta) \sin 0 \cos 0\, d0\, d\beta. \qquad (2)$$

on the basis of a single measured value of the intensity of reflected radiation $J(\theta^*,\beta^*)$ for zenith angle θ^* and azimuth β^* (the azimuth is usually figured from the Sun's direction).

If this operation is carried out, the albedo A_s of the Earth-atmosphere system is determined from the following obvious equation: /32

$$A_s = \frac{F}{S_0 \cos i}, \qquad (3)$$

where S_0 is the solar constant and i is the Sun's unit angle.

The idea behind all conversion methods lies in the use, directly or indirectly, of data on the average angular distribution of the scattered (emergent short-wavelength) radiation. The conversion reduces to the use of the hypothesis of isotropy of the radiation field or the angular distribution data obtained on the basis of theoretical calculations for a "climatic" model of the atmosphere. Data from direct measurements, namely, satellites, balloons, and airplanes, have also been applied in a number of papers [40, 41].

Let the function $X(\theta^*,\beta^*,i)$ be defined with respect to the angular distribution of the average intensity of scattered radiation $\bar{J}(\theta,\beta,i)$ as follows:

$$X(\theta^*,\ \beta^*,\ i) = \frac{\pi \bar{J}(\theta^*,\ \beta^*,\ i)}{\int_0^{2\pi} \int_0^{\frac{\pi}{2}} \bar{J}(0,\ \beta,\ i) \sin 0 \cos 0\, d0\, d\beta}. \qquad (4)$$

Apart from the angle θ^* and β^*, the fraction of the radiation scattered in different directions still depends on the Sun's zenith angle i, i.e., X is a function of three variables. If $J(\theta^*,\beta,i)$ is the result of a measurement of a radiation intensity of a specific geographical point, the albedo of the Earth-atmosphere system at this point is equal to

$$A_s = \frac{\pi J(\theta^*, \beta^*, i)}{S_0 \cos i X(\theta^*, \beta^*, i)} . \qquad (5)$$

An attempt to reduce the data of Nimbus II and Nimbus III showed [40, 41] that the use of the results of "model" calculations for determining the function of X does not lead to satisfactory results. The construction of typical angular distributions of the emergent short-wavelength radiation on the basis of the experimental data is significantly more reliable. The authors of [40], for example, used three characteristic angular distributions for the solar zenith angle ranges of 0-35, 35-60, and 60-80°.

The corresponding conversion procedure for measurements in the long--wavelength spectral region turns out to be simpler, since the angular distribution of the emergent thermal radiation does not depend on the average either on the Sun's altitude or on its azimuth (of course, the angular distribution is very "mottled" in the presence of frequent cloudiness). Therefore, it turns out to be sufficient to introduce a characteristic of the average angular distribution of the emergent long-wavelength radiation /33 Y(θ*) as follows:

$$Y(\theta^*) = \frac{\bar{J}(\theta^*)}{2\int_0^{\frac{\pi}{2}} \bar{J}(\theta) \sin\theta \cos\theta \, d\theta}, \qquad (6)$$

which permits reducing the measured values of the radiation intensity J(θ*) to fluxes F:

$$F = \frac{\pi J(\theta^*)}{Y(\theta^*)} . \qquad (7)$$

Just as in the determination of the function X, the statistical reduction of empirical data on the emergent long-wavelength radiation is the most reliable method of finding the function Y.

The reduction to the level of the atmosphere's nominal upper boundary of the flux values measured by wide-sector (hemispherical) radiometers for the long-wavelength spectral region also turns out to be very simple.

Since a dependence of the long-wavelength emergent radiation's angular distribution on azimuth is absent on the average and the radiation vector is directed along a radius from the Earth's center, we have

$$F(h) = F(H)\left(\frac{a+H}{a+h}\right)^2, \qquad (8)$$

where a is the Earth's radius, H is the satellite's altitude, and h is the altitude of the atmosphere's nominal upper boundary.

In the case of short-wavelength radiation the method for determining the albedo of the Earth-atmosphere system from the data of wide-angle radiometer measurements should also both take into account the nonuniformity of the sighted territory's illumination by the Sun and take into detailed account the average angular distribution of the scattered radiation.

It is necessary to turn our attention also to the problems of spatial localization and the accuracy of interpreting the data of the wide-angle radiometer measurements. These problems were discussed by K. Ya. Vinnikov [46]. He showed that the data of similar measurements were treated incorrectly in a number of papers as the average values of the radiation fluxes over the entire survey area, which at the normal altitudes of meteorological satellite amounts to about 7% of the Earth's surface.

Using the results of investigations of the statistical structure of radiated fluxes, one can show that the data of the hemispherical radiometers should be interpreted as average values over comparatively small areas. The measurable values of the long-wavelength emergent radiation differ, according to the estimates of K. Ya. Vinnikov, least of all (in the sense of a minimum of the mean square error) from the values of the radiation averaged over a circular area with its center at the subsatellite point and having a radius of /34
750, 1,100 and 1,400 km at satellites, altitudes of 500, 800 and 1,000 km, respectively. Regardless of the large scale of the spatial averaging carried out by the wide-angle radiometers, they capture a significant fraction of the emergent radiation field's dispersion (74, 63, and 55%, respectively at

the satellite altitudes indicated above). The latter situation can be explained only by the exceptionally large scale of the main perturbations of the long-wavelength emergent radiation field.

The indication is that the data of measurements carried out with the help of wide-sector radiometers is of great information content (and of sufficiently concentrated localization).

Taking into account the diurnal variation of the components of the radiation balance of the Earth-atmosphere is an important step in the data reduction. This must be considered first of all in order to make the data of measurements over a large territory comparable.

The effect of the diurnal variation can be excluded by replacing the measured flux values by conditional diurnal sums (see [61]). We will designate as conditional diurnal sums the diurnal sums of the radiation obtained on the basis of a single measurement on the assumption that only the Sun's altitude but not the atmosphere's parameters and its surface have a diurnal variation. Account of the diurnal variation has been carried out most completely in [39-41], which are devoted to a climatological reduction of the data of the Nimbus II and Nimbus III satellites. Since these satellites were located in a solar-synchronous orbit, i.e., all the measurements were carried out at midnight or noon according to local mean polar time at any geographical point, consideration of the diurnal variation was especially important for the short-wavelength radiation, all measurements of which refer to the Sun's maximum altitude.

In the course of the reduction of the Nimbus II data [39] an empirical dependence was constructed of the albedo of the Earth-atmosphere system on the Sun's zenith angle. This empirical dependence was then used to calculate the albedo, which is definable as the ratio of the amount of radiation reflected during the daylight hours to the diurnal sum of solar radiation arising at the atmosphere's upper boundary.

It was later shown [41] that the use of a single universal dependence of the albedo on the Sun's zenith distance does not lead to sufficiently correct results. Therefore, in the reduction of the Nimbus III data two

characteristic dependences were used (Figure 14): one of these dependences was for an underlying surface with low albedo (ocean), and the other was for surfaces with high albedo (clouds or dry land). Consideration of Figure 14 clearly demonstrates the importance of differentiating the dependence of the albedo on the Sun's zenith distance. The use of these data have led the values of the albedo for the oceans which are somewhat higher than those obtained in the reduction of the Nimbus II results. On the contrary, the values of the albedo over regions of dry land, cloudiness, and snow cover were decreased somewhat. Partially in connection with this situation, the global albedo based on the Nimbus III data turned out to be 1-2% lower than /35
that based on Nimbus II data (see below).

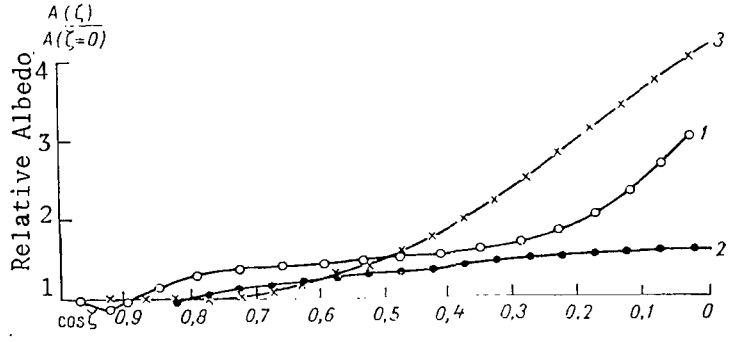

Figure 14. Dependence of the Albedo of the Earth-Atmosphere System on the Sun's Altitude ζ.
1 -- Universal dependence taken in the reduction of the Nimbus II data;
2 -- Dry land and clouds (Nimbus III); 3 -- Ocean (Nimbus III).

The radiation characteristics obtained as a result of the reduction stages enumerated should undergo an objective analysis. Since in the majority of contemporary methods of numerical weather prediction information is used which is interpolated provisionally at the nodes of a regular grid, it is necessary to solve the analogous problem for the radiation fields.

In contrast to such meteorological elements as the geopotential, temperature, pressure, and wind (for which local values of the elements themselves or their differential characteristics should be obtained at the

nodes of a regular grid as the result of interpolation), the notion of obtaining interval characteristics arises when dealing with the radiation fluxes.

As K. Ya. Vinnikov has shown [48], it is advisable to carry out the analysis in such a way as to obtain values of the emergent radiation or albedo averaged over areas of elementary squares of a regular grid.

In the reduction of the data of measurements made with the help of the Tiros satellites a very simple method was used by the American investigators to obtain such integral characteristics in the neighborhood of each node of a square grid with an increment of about 350 km [62]. Evidently the method of optimal averaging of random quantities proposed by R. L. Kagan [47] is more ideal in the present case. The possibilities and peculiarities of the application of this method to an analysis of the field of actinometric quantities have been discussed in detail by K. Ya. Vinnikov [48].

The main idea of the method of optimal averaging lies in the following.

The average value of an element q_0 over a square whose side is l, namely, /36

$$q_0 = \frac{1}{l^2} \int_{-\frac{l}{2}}^{\frac{l}{2}} \int_{-\frac{l}{2}}^{\frac{l}{2}} q(x, y)\, dx\, dy \tag{9}$$

is sought in the form of a linear combination of values of the elements q_i at n point, which can be located both inside the square and outside it,

$$q_0 \approx \tilde{q}_0 = \sum_{i=1}^{n} p_i q_i. \tag{10}$$

The weight coefficients with which the values of the element q_i enter at each of the n points are determined by the method of least squares from the condition of a minimum of the mean square error of the representation given in equation (10).

The values of the autocorrelation function of the field of the element being analyzed are the coefficients of the system of linear algebraic

equations for determining the interpolation weights p_i in the case of such a statement of the problem, and the righthand sides of these equations are the values of the reciprocal correlation function between the average and local values of the same element.

The problem of investigating the statistical structure of the radiation fields arises in connection with the solution of the problem of objective analysis. Some results in this direction have already been obtained in the papers of E. P. Borisenkov, Yu. P. Doronin, and K. Ya. Kondrat'ev [63, 64], L. S. Gandin and V. P. Boltenkov [65], and others.

Application of statistically optimal methods of analysis permits compressing the volume of information which enters as a result of the measurements by virtue of the filtering out of random fluctuations of the radiation field which do not have predictive or diagnostic value. The integral characteristics of the radiation fields are more convenient in comparison with local characteristics in the investigation of large-scale processes in the atmosphere, the energy balance of the Earth-atmosphere system, and also for climatological generalizations.

Mean Annual Planetary Distribution

Until recently our ideas about the regularities of the planetary distribution of the radiation balance of the Earth's surface-atmosphere system were based almost exclusively on the use of calculated data [51-56].

The actinometric data of meteorological satellites first permitted us to carry out a comparison with experiment of the computed climatological map of the planetary distribution of radiation balance of the Earth's surface-atmosphere system. However, at the first stage of the investigations such a comparison could be only rather tentative, since the experimental data were restricted from the point of view of the possibility of their /37
adequate spatial-temporal averaging. Only in recent papers [39-44, 80] are results being published of a reduction of satellite actinometric information which represent the correct climatological properties (average values during a year, the seasons, and months) referring to practically the entire Earth. These data have set up the basis for the first investigations in the region

of satellite radiation climatology and have permitted carrying out a check of the results of calculations which were made earlier.

In the comparison carried out by K. Ya. Kondrat'ev and L. N. D'yachenko [49], they used the data of calculations and maps of the planetary distribution of the Earth's radiation balance and its components obtained in the papers of T. G. Berlyand [51], K. Ya. Vinnikov [52-53], K. Ya. Kondrat'ev, L. N. D'yachenko, and K. Ya. Vinnikov [45], and A. Katayama [54]. The results of satellite measurements (during the period of July 1963 until November 1965) reduced by T. H. Vonder Haar [42] were the source of the experimental data.

T. H. Vonder Haar used very extensive satellite actinometric information obtained with the help of the y-angle detectors of V. E. Suomi's system, and he applied a sufficiently correct procedure for reducing the results of the measurements, taking into account the data of frequent onboard calibrations based on the Sun. This procedure gave a basis for the assumption that the effect of random pairs was practically excluded. The errors in determining the average values of the radiation balance and its components do not exceed several percent.

A comparison of the experimental annual maps of the planet's radiation balance R_s with the computed climatological maps shows that completely satisfactory qualitative agreement is observed for the fields of the radiation balance (Figure 15). For example, the zones of maximum values of the balance, which are located in the region of equatorial latitudes, match. However, as far as the absolute value is concerned, the calculated values R_s are significantly smaller than the measured values. As the latitude increases, a decrease is observed in the radiation balance; the zero isolines (calculated and measured) are located nearby the latitude 40° both in the southern and northern hemisphere. The distribution of the balance in the southern hemisphere is almost zonal, which is caused by the uniformity of the underlying surface (ocean).

The agreement of the zero isolines of the balance is satisfactory enough. The largest deviation occurred on dry land, in the region of the southern extremity of the South American continent. In the Northern Hemisphere the

deviation of the zero isolines is also small over the ocean and significant over the continents. The calculated zero isoline deviates particularly strongly only from latitude 40° and from the isoline based on the measured data over part of the Eurasian continent.

The nonuniformities of the underlying surface of the continents result in a mismatch of the isolines of the measured and calculated values of the radiation balance, which is especially noticeable in the region of the /38
Sahara and Arabian deserts. The minimum values of R_s occur in the polar regions of the northern and southern hemispheres. The measured values of R_s vary from values smaller than -0.08 to +0.12 cal/cm^2·min in the Northern Hemisphere and from -0.12 to +0.12 cal/cm^2·min in the Southern Hemisphere (see Figure 15), and the calculated values vary from -0.12 to +0.08 cal/cm^2·min in the Northern Hemisphere and from -0.04 (the region of 50° S. Lat.) to +0.08 cal/cm^2·min in the Southern Hemisphere.

Success in obtaining data for the calculations of R_s for higher latitudes than 50° S. Lat. has not been achieved because of the absence of the necessary initial information.

It is natural that the nature of the geographical distribution of the radiation balance of the Earth-atmosphere system is determined by the specific properties of the spatial variability of its components, namely, the planet's albedo A_s and the emergent long-wavelength radiation F_∞.

Upon comparison of the annual map of the Earth-atmosphere system's albedo constructed by T. H. Vonder Haar on the basis of satellite measurements with the climatological map of K. Ya. Vinnikov, attention is drawn first of all to the systematic quantitative discrepancy, which amounts to approximately 17° on the average for the entire Earth (Table 1). The calculated values of the albedo for all the latitude belts systematically exceed the measured values. Evidently, this situation is explained in the first place by an exaggeration in the estimate of the amount and density of the clouds utilized for the albedo calculations. It is possible that the strongly expressed /39
"topography" of the convective cloudiness of low latitudes also plays a certain role. The large-scale roughness of the cloud cover can result in a noticeable decrease of the Earth's albedo.

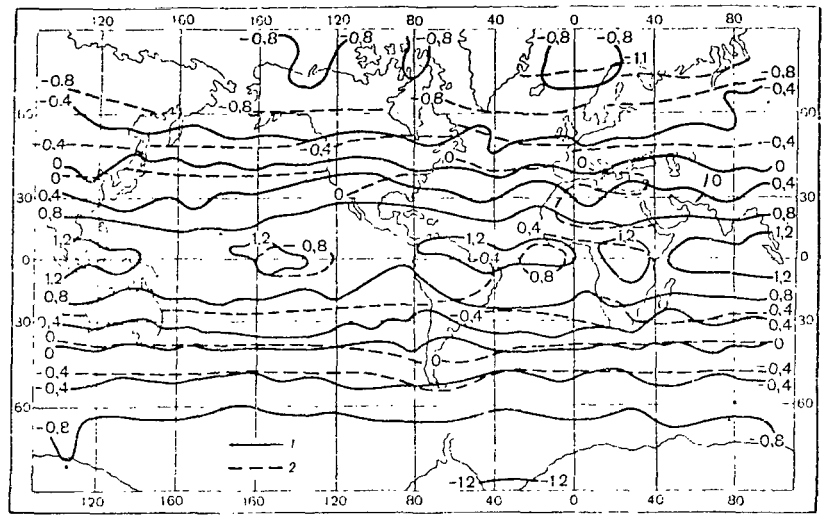

Figure 15. Average Radiation Balance of the Earth-Atmosphere System During the Year (cal/cm^2·min).
1 -- Measured values; 2 -- calculated values. Note: commas indicate decimal points.

TABLE 1

AVERAGE VALUES DURING THE YEAR OF THE EARTH-ATMOSPHERE SYSTEM'S RADIATION BALANCE AND ITS COMPONENTS FOR DIFFERENT LATITUDE BELTS.

Latitude, Degrees	A%		F_∞ cal/cm^2·min		R_s cal/cm^2·min	
	Calc.	Meas.	Calc.	Meas.	Calc.	Meas.
80-70 N.	--	44	--	0.24	--	-0.10
70-60	43	40	0.27	0.27	-0.09	-0.07
60-50	40	36	0.29	0.29	-0.06	-0.05
50-40	37	32	0.30	0.31	-0.02	0.00
40-30	35	27	0.32	0.34	0.01	0.02
30-20	33	24	0.34	0.38	0.03	0.04
20-10	32	20	0.35	0.38	0.04	0.09
10-0	33	20	0.34	0.38	0.06	0.11
0	33	20	0.34	0.38	0.06	0.10
0-10 S.	33	20	0.34	0.37	0.06	0.10
10-20	33	20	0.34	0.38	0.05	0.08
20-30	33	23	0.33	0.38	0.04	0.06
30-40	35	27	0.31	0.34	0.02	0.03
40-50	38	32	0.29	0.31	-0.02	-0.01
50-60	--	36	--	0.29	-0.05	-0.06
60-70	--	40	--	0.27	--	-0.09
70-80	--	45	--	0.23	--	-0.11
Earth	35	29	0.32	0.33	-0.03	+0.04

Another difference consists of the fact that if a gap at the boundary of dry land and the sea is characteristic for the calculated isolines, the measured values do not experience such a gap (Figure 16), which, of course, is caused by the large spatial averaging.

Examination of the annual map of the albedo (Figure 16) shows that significant deviations from zonality are observed only in the near-equatorial zone. The largest values of the albedo occur at high latitudes (beyond the north and south polar circles), and the minimum values occur in the near--equatorial zone over the ocean.

The distinctive features of the emergent long-wavelength radiation field are characterized by the map illustrated in Figure 17. A significant non-zonality is observed in this case only in the near-equatorial zones. The quantitative deviations of the measured and calculated values of the emergent radiation (see Table 1) is significantly smaller than in the case of the albedo. The measured values exceed somewhat the calculated values in temperate and tropical latitudes, but north of 50° N. Lat. the deviations are practically insignificant. In practice, the average calculated and measured values of the emergent radiation for the entire Earth coincide /40 (0.32-0.33 cal/cm^2·min).

J. London and T. Sasamori [55] have completed new calculations of the average annual meridional profiles of the Earth-atmosphere system's radiation balance, which has also made it possible to find more exact values of the thermal balance of the Earth as a whole. The use of a more refined procedure in the calculations and of far more complete original meteorological data has permitted obtaining results which are in very good agreement with experiments (only an insignificant adjusting of components of the balance, for example, expressed as an increase by 1% of the absorbed solar radiation, was carried out to provide a zero average annual radiation balance of the Earth as a whole).

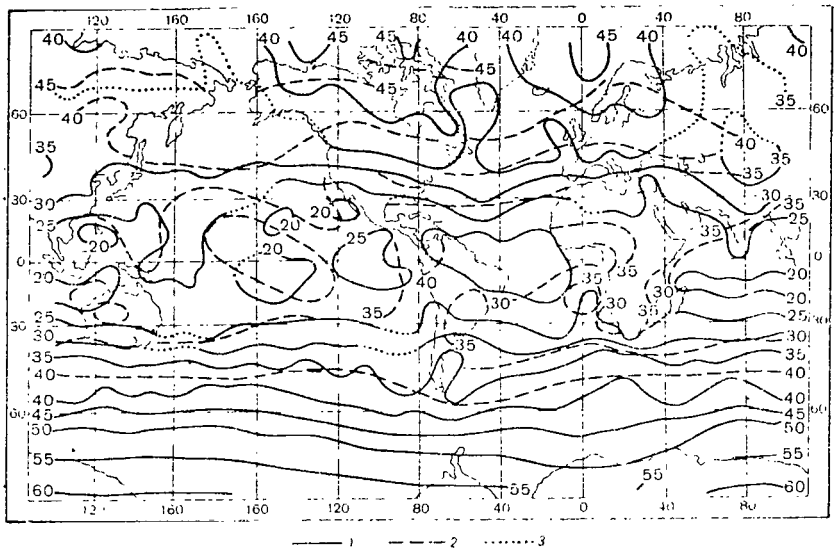

Figure 16. Average Albedo of the Earth-Atmosphere System During the Year (%).
1 -- Measured values, 2 -- calculated values, 3 -- gap.

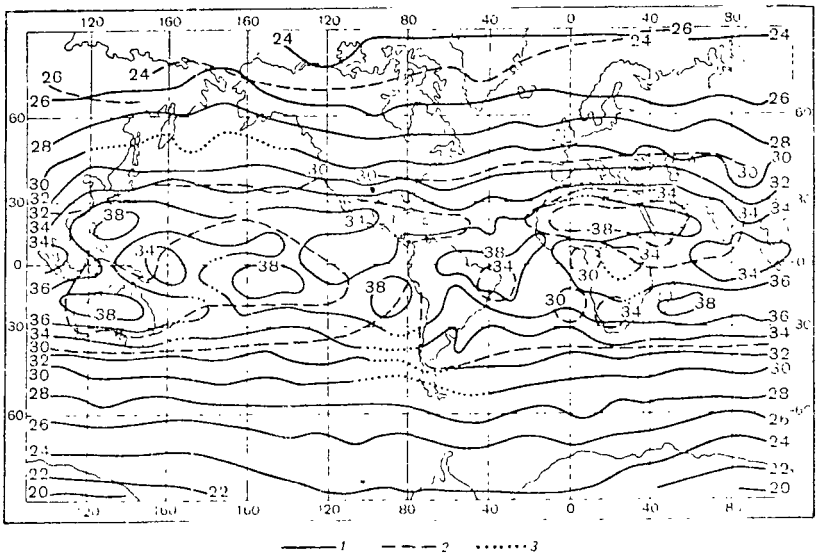

/41

Figure 17. Emergent Radiation (cal/cm^2·min).
1 -- Measured values, 2 -- calculated values, 3 -- gap.

The layout of the global distribution of the average annual values of the radiation balance proposed by J. London and T. Sasamori [55] is presented in Figure 18. The average arrival of solar radiation outside the atmosphere's boundaries, which is equal to 1/4 S_0, is taken as 100%. The Earth's average albedo amounts to 33% and is determined first of all by the reflection of radiation by the clouds (26%). Reflection by the underlying surface and scattering (back) by the cloudless atmosphere makes a far smaller contribution (7%). Since the average degree of cloudiness for the Earth is equal to approximately 50% as a whole, it is easy to understand that the average albedo of the clouds amounts to 50%, and the albedo of the cloudless part of /42
the planet amounts to about 15%. These results practically correspond to the range of albedo obtained by E. Raschke and W. Bandeen [40] from the Nimbus II data (with S_0 = 1.95 cal/cm^2·min, these authors obtained a value of the Earth's albedo equal to 31%). Absorption of radiation by the atmosphere (both molecular, which is caused by absorption by water vapor, ozone, carbon dioxide gas, and oxygen, as well as aerosol absorption, which is due to the clouds and dust) is equal to 22%, which causes radiation heating of the atmosphere amounting to 0.6 degrees/day. Approximately one-half of the absorption is due to the water vapor fraction. The underlying surface absorbs 45%. This absorption is distributed in almost equal parts between direct solar (24%) and scattered (21%) radiation.

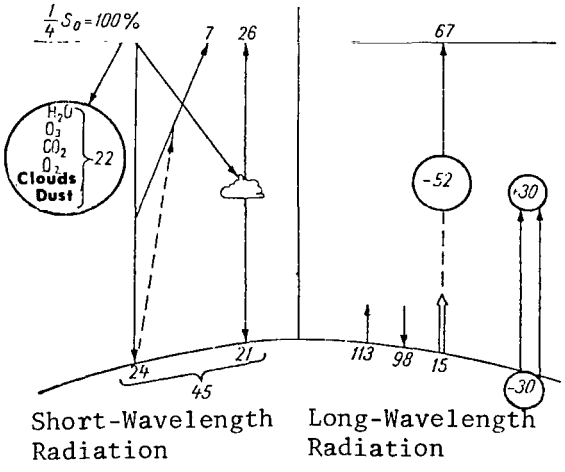

Figure 18. Average Annual Radiation Balance of the Earth as a Whole (in % with Respect to the Average Arrival of Solar Radiation Outside the Atmosphere's Boundary).

The values of the long-wavelength emergent radiation F_∞ and the effective radiation of the underlying surface F_0 amounts to 67% and 15%, respectively, which causes a negative long-wavelength balance of the atmosphere equal to 52%. This situation means that radiation cooling reaches 1.5 degrees/day. Such cooling is almost two-thirds compensated by the heat of condensation of water vapor (30%), while the contribution due to the absorption of solar radiation is equal to 22%. The effective radiation is formed as the difference of the underlying surface's own radiation (113%) and the counter-radiation of the atmosphere (98%). If one takes S_0 = 2 cal/cm^2·min, the absolute value of F_∞ = 0.335 cal/cm^2·min, which corresponds to a radiation temperature of about 253°K (this value very nearly agrees with that obtained from satellite measurements) [sic].

Analysis of the computational data showed that on the average the radiation balance is close to zero during the year in both hemispheres. However, in the Southern Hemisphere higher values of the albedo and smaller values of the emergent radiation occur than in the Northern Hemisphere. These differences are fixed first of all by the more significant cloudiness in the Southern Hemisphere.

The results of measurements according to T. H. Vonder Haar and of calculations of the average meridional profiles of the emergent long-wavelength radiation and the absorbed solar radiation are presented in Figure 19. As is evident, agreement of the results of the calculation with the data of the measurements turned out to be completely satisfactory. It is possible that the small underestimation of the values of the emergent radiation and the absorbed radiation in the Southern Hemisphere is caused by an overestimation of the degree of cloudiness taken in the calculations (data on the climatology of cloud cover are still not adequate, especially from the point of view of determining the type and altitude of the clouds). The zone of positive values of the radiation balance includes a band from 33° N. Lat. to 37° S. Lat.

One of the important and interesting properties of the Earth's radiation balance is the atmosphere's long-wavelength balance or the inflow of heat to the atmosphere's entire thickness because of the long-wavelength component

of the radiation balance. It represents the difference between the effective radiation of the underlying surface and the emergent radiation, namely, $F_a = F_0 - \overline{F}_\infty$. The long-wavelength balance is always negative, and this indicates that the atmosphere as a whole is cooled because of the long- /43
-wavelength radiation.

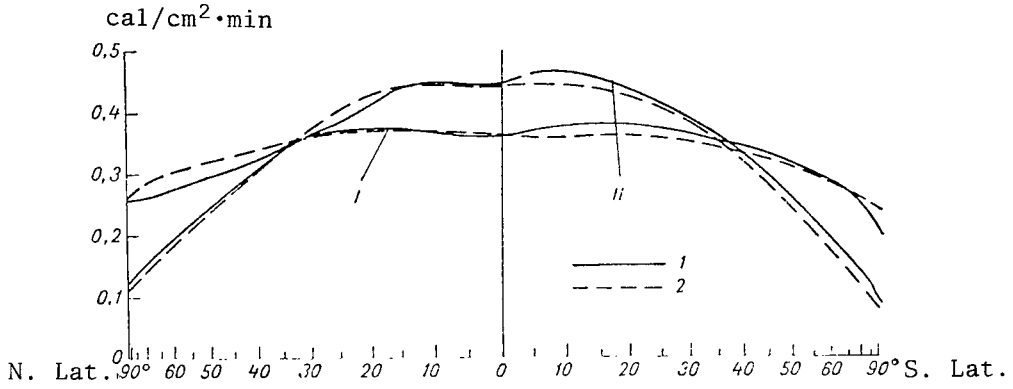

Figure 19. Annual Average Meridional Profiles of the Emergent Long-Wavelength Radiation (I) and the Absorbed Solar Radiation (II). Note: commas indicate decimal points. 1 -- Measured values, 2 -- calculated values.

As an example of the distribution over the Earth of the atmosphere's long-wavelength balance F_a, a map of the annual sum (kcal/cm²·year) constructed by L. N. D'yachenko and K. Ya. Kondrat'ev [56] is presented in Figure 20.

The extreme insufficiency of the data of measurements of the atmosphere's long-wavelength balance has acted as a stimulus to taking up the solution of the problem of establishing correlation dependences between the values of /44 the emergent radiation F_∞ and the long-wavelength balance F_a [57, 58]. It is difficult to overestimate the importance of such dependences, since they make it possible to derive the quantitative characteristics of the atmosphere's long-wavelength balance from values of F_∞ measured, for example, with the help of meteorological satellites or actinometric radiosondes.

The connection between the atmosphere's long-wavelength balance F_a and the emergent radiation F_∞ (radiation probe) was found to be non-unique. The

authors of [59] therefore attempted to analyze it for separate points under various sky conditions (clear, hazy). In addition, warm and cold periods were also treated separately (winter, summer).

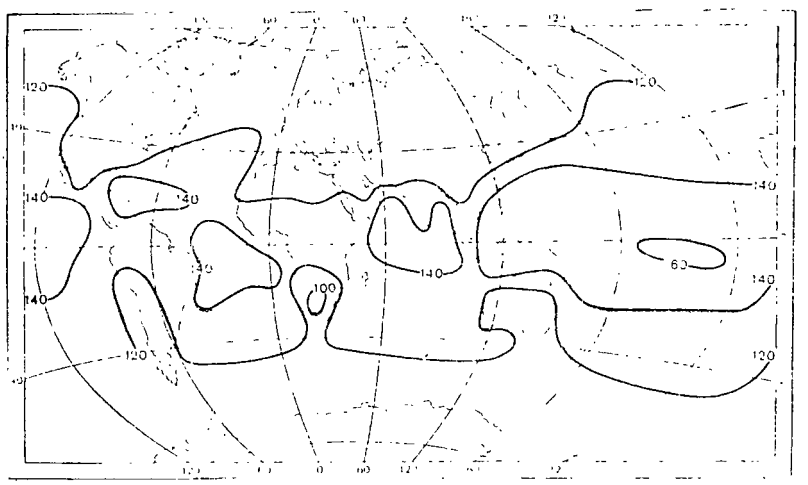

Figure 20. Average Annual Long-Wavelength Balance of the Atmosphere (kcal/cm^2· ·year).

It turned out that with such differentiation the dependence of F_a on F_∞ is sufficiently distinct. A particularly high coupling is observed in the case of continuous low cloudiness of the FrNb, Ns, Cb type, when the defective radiation from the Earth's surface was practically equal to zero.

Empirical equations for the cases of clear and hazy weather were obtained from the data of actinometric radiosondes on the basis of the use of the correlation dependences. These equations have the form (r is the correlation coefficient):

Hazy (10 Points)

Summer $F_a = 1.05F_\infty - 0.018$; $r = 0.99$

Winter $F_a = 1.18F_\infty - 0.048$; $r = 0.98$

Clear (0-2 Points)

Summer $F_a = 1.44F_\infty - 0.199$; $r = 0.92$

Winter $F_a = 1.43F_\infty - 0.143$; $r = 0.89$.

L. V. Berkovich [59] obtained the following regression equations for the /45
thermal period on the basis of data of measurements of the Kosmos-144 satellite:

Clear (0-2 Points) . . $F_a = 0.081F_\infty - 0.217$; $r = 0.68$

All Cases of Cloudiness

(0-10 Points) . . $F_a = 0.440F_\infty - 0.160$; $r = 0.26$.

The regression equations obtained by various authors are presented in Table 2. It is natural that the large variety of correlation relations hinders the practical solution of the problem of utilizing the data of measurements of the long-wavelength emergent radiation for determining the atmosphere's long-wavelength balance. However, the urgency of this problem requires carrying out similar subsequent investigations on the basis of the use of more extensive observational data.

TABLE 2

CORRELATION RELATION BETWEEN THE ATMOSPHERE'S LONG-WAVELENGTH BALANCE AND THE EMERGENT RADIATION. SUMMER.

Authors	Cloudiness	Correlation Coefficient	Regression Equation	Source of Measurement Data
K. Ya. Kondrat'ev and L. N. D'yachenko	0-2 Points	0.92	$F_a = 1.44F_\infty - 0.20$	Radiosonde
R. R. Sabatini and V. E. Suomi	Clear	0.87	$F_a = 1.54F_\infty - 2.34$	Artificial Earth Satellite
L. V. Berkovich	0-2 Points	0.68	$F_a = 0.08F_\infty - 0.22$	Artificial Earth Satellite
K. Ya. Kondrat'ev and L. N. D'yachenko	Hazy (10 Points)	0.99	$F_a = 1,05F_\infty - 0.02$	Radiosonde
R. R. Sabatini and V. E. Suomi	Hazy	0.85	$F_a = 1.32F_\infty - 0.13$	Artificial Earth Satellite
L. V. Berkovich	All Cases (0-10 Points)	0.26	$F_a = 0.44F_\infty - 0.16$	Artificial Earth Satellite

Planetary Distribution for Comparatively Short Time Intervals

The reduction of results of measurements of emergent radiation made with the help of narrow-angle radiometers have permitted investigating the peculiarities of the global fields of the Earth-atmosphere system's radiation balance and its components during short time intervals (the averaging was carried out mainly over three-month and two-week intervals).

The first detailed investigations in this direction were carried out by J. S. Winston [37], who constructed on the basis of Tiros IV and Tiros VII satellite data maps of the geographical distribution of the radiation balance and its components for the individual months and all the seasons. The large-scale peculiarities of the field of the radiation balance (which is determined in the first place by the cloudiness conditions) are always sufficiently characteristic. The presence of broad maxima is typical for the long-wavelength emergent radiation in the tropics or the subtropics of both hemispheres, between which is located a belt of lower values of the emergent radiation associated with the intertropical convergence zone (Figure 21). The strongest decrease of the emergent radiation with increase in latitude occurs in the 20-50° latitude belt, and the latitudinal gradient of the emergent radiation varies as a function of the time of year.

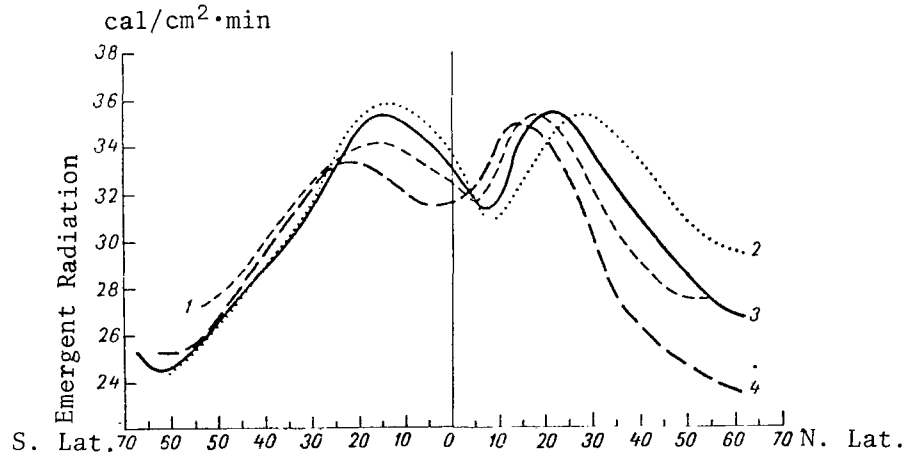

Figure 21. Meridional Profiles of the Long-Wavelength Emergent Radiation at Various Times of Year.
1 -- March-May 1962, 2 -- June-August 1963, 3 -- September-November 1963, 4 -- December 1963 - February 1964.

The latitudinal dependence of the albedo represents as a rule a mirror image of the latitudinal variability of the emergent radiation (Figure 22), since cloudiness is also the main factor which determines the variation of the albedo (but in the opposite direction). Desert regions, where high values of the albedo are accompanied by large values of the emergent radiation (due to the high temperature of the underlying surface and the small amount of clouds), comprise an exception. Other exceptions are observed. Thus, for example, in March-May 1962 a maximum of the albedo occurred to the south- /46
west of California in the case of a very significant emergent radiation. This case should be ascribed to the effect of the stable cloudiness of the lower level.

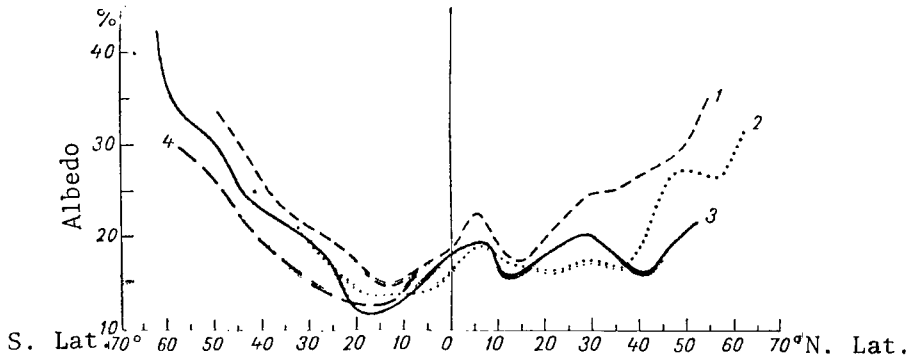

Figure 22. Meridional Profiles of the Albedo at Various Times of the Year.
Notation same as in Figure 21.

The data of T. H. Vonder Haar and V. E. Suomi [44] are presented in Figure 23. These data characterize the average meridional profiles of the radiation balance at various times of year and illustrate the fact that a strong increase in the amplitude of the annual variation of the radiation balance occurs as the latitude increases. The sharpest variation in the nature of the meridional profile of the radiation balances are observed upon the transition from summer to fall.

The most detailed investigations of the global fields of the radiation /47
balance and its components have been carried out in recent years on the basis of the Nimbus II and Nimbus III satellite data [39-41]. The Nimbus II

data have permitted constructing world maps of the distribution of the radiation balance and its components over five consecutive two-week time intervals during the period from May 16 through July 28, 1966. The spatial resolving power of the five-channel radiometer mounted on Nimbus II varied from 50 km (near the subsatellite point) to 110 km (at a nadir angle of 40°). The accuracy of the measurements was about ±2%. The scale of averaging (in mapping the results) decreased from 560 × 560 km at the Equator to 280 × 280 km at a latitude of 60°. All the calculations were made on the assumption that the solar constant is equal to 2 cal/cm^2·min.

The latitude-time cross sections obtained by E. Raschke and V. Bandeen [40], which illustrate the peculiarities of the meridional profiles of the albedo A, the emergent radiation F_∞, the radiation balance R_s, and the arrival of solar radiation outside the atmosphere's boundary Q_0 at various periods of time (all the quantities are expressed in cal/cm^2·min), are reproduced in Figure 24.

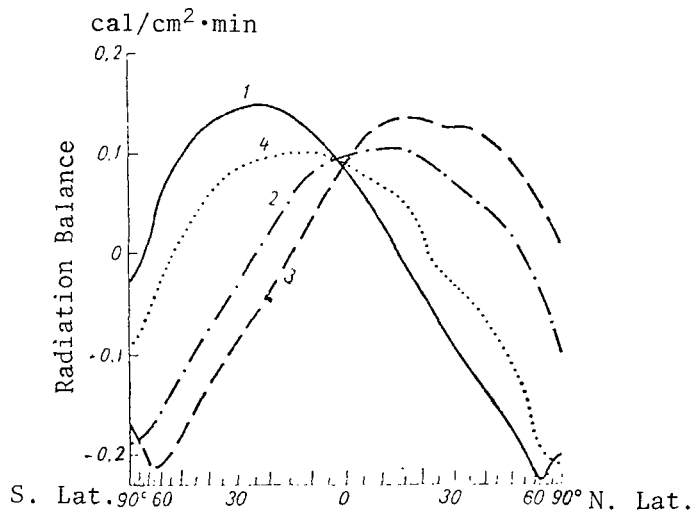

Figure 23. Meridional Profiles of the Radiation Balance at Various Times of the Year.
1 -- Winter (December, January, February), 2 -- Spring (March, April, May), 3 -- Summer (June, July, August). 4, Autumn (September, October, November).
Note: commas indicate decimal points.

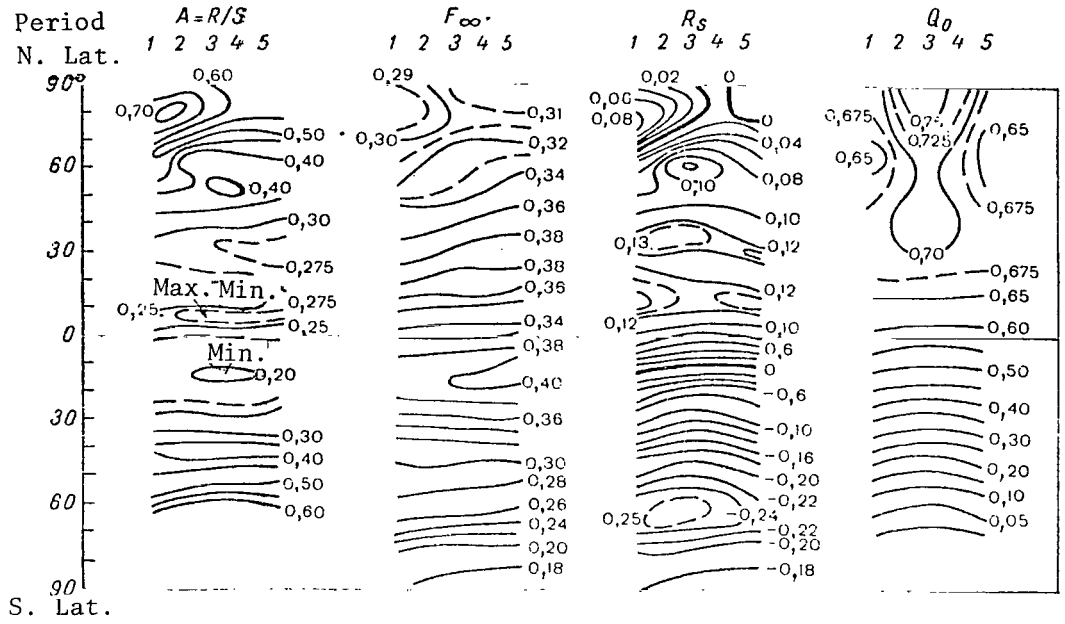

/48

Figure 24. Latitude-Time Cross Section of the Two-Week Average Values of the Radiation Balance and Its Components. Note: commas indicate decimal points.

An analysis of the data of Figure 24 and the maps mentioned above shows that the main peculiarities of the albedo field are sufficiently stable in time. Albedos greater than 55% are observed only over the Arctic ice cap and snow cover, especially in May, when the albedo of the polar cap amounts to /49 about 75%, decreasing (as the snow and ice melt) to 60% in July. The high values of the albedo of the Greenland glacier (75-80%) are steadily maintained during the year. As the latitude decreases, the albedo decreases to values less than 20% over the sparsely clouded regions of the subtropics. The albedo of the cloudless deserts of Africa and Arabia reach values which exceed 35%.

The variability of the emergent radiation reflects the peculiarities of the latitudinal variation already discussed above. We only note that the absolute minimum of the emergent radiation is recorded over Antarctica.

Only during the period of July 1-15, 1966 over the central Arctic did a weak positive radiation balance occur ($R_s < 0.03$ cal/cm^2·min). During this

period Greenland was a region of negative radiation balance (to -0.12 cal/cm^2··min), which is caused by the large albedo. During the course of the entire 2.5-month period a zone of positive balance covered the Northern Hemisphere south of 70-75° N. Lat. and the band 0-10° S. Lat. The maximum of the radiation balance is observed over the northern part of the oceans of the subtropics (the low albedo of the oceans has decisive significance). Almost--zero values of the balance (small negative values were observed sometimes) are characteristic for the large deserts of North Africa and Arabia.

The estimates of the radiation balance and its components for the hemispheres and the entire Earth carried out on the basis of Nimbus II and Nimbus III data are of great interest. The Nimbus II data are presented in Table 3 obtained by E. Raschke and V. Bandeen [40]. As is evident, the Earth's albedo varies during the period under consideration within the limits of 29-31%. The albedo of the Southern Hemisphere is noticeably smaller during this period than the albedo of the Northern Hemisphere, in connection with the fact that Antarctica, with its high albedo values, is located in the zone of polar night and therefore does not introduce its contribution to the albedo of the Southern Hemisphere. We note that if, for example, we take S_0 = 1.95 cal/cm^2·min, the Earth's albedo is equal to 30.9% during the period June 16-30.

The Earth's radiation temperature undergoes small variation (254-255°K). The Northern Hemisphere is approximately 3°K warmer than the southern hemisphere. The global radiation balance has mainly (with the exception of the time from May 16-31) a negative sign, and it is essentially less than -0.01 cal/cm^2·min (in the case of S_0 = 1.95 cal/cm^2·min it amounts to a value of -0.02 cal/cm^2·min for the June 16-30 period). This situation is determined by the fact that the negative balance of the Southern Hemisphere is not compensated by the positive balance of the Northern Hemisphere.

A somewhat more correct reduction of the Nimbus III data [41] for June 16-30 and July 1-15, 1969 gave albedo values of 29 and 31%, respectively, values of 0.330 and 0.338 cal/cm^2·min for the emergent radiation (which corresponds to radiation temperatures of 252-253°K), and values of the Earth's

radiation balance of +0.002 and -0.004 cal/cm^2·min (in the case under discussion S_0 = 1.95 cal/cm^2·min is taken). The global distributions of the radiation balance on the basis of the Nimbus II and Nimbus III data are very similar, with the exception of the fact that in the last case positive values of the radiation balance were obtained for the regions of the Sahara, Greenland, and the Arctic. /50

TABLE 3

RADIATION BALANCE OF THE EARTH-ATMOSPHERE SYSTEM AND ITS COMPONENTS FOR THE SEPARATE HEMISPHERES AND THE ENTIRE EARTH BASED ON THE NIMBUS-II DATA.

Period of the Measurements, 1966	Hemisphere	Q	R	A	T_r	F_∞	$Q-R$	R_s
May 16-31	N	0,659	0,216	32,8	255,2	0,345	0,443	+0,098
	S	0,316	0,078	24,7	252,7	0,333	0,238	—0,095
	W	0,488	0,147	30,1	251,0	0,339	0,341	+0,002
June 1-15	N	0,671	0,221	32,8	256,0	0,350	0,453	+0,103
	S	0,297	0,076	25,6	253,2	0,334	0,221	—0,113
	W	0,486	0,149	30,6	254,8	0,342	0,337	—0,005
June 16-30	N	0,676	0,217	32,1	256,5	0,353	0,459	+0,106
	S	0,291	0,074	25,4	253,5	0,336	0,217	—0,119
	W	0,484	0,146	30,1	255,2	0,345	0,338	—0,007
July 1-15	N	0,670	0,210	31,4	257,0	0,356	0,460	+0,104
	S	0,298	0,072	24,1	253,5	0,336	0,226	—0,110
	W	0,484	0,141	29,1	255,2	0,346	0,343	—0,003
July 16-28	N	0,653	0,203	31,1	256,8	0,355	0,450	+0,095
	S	0,317	0,084	26,5	253,2	0,334	0,233	—0,101
	W	0,485	0,143	29,5	255,2	0,345	0,342	—0,003

The absolute values of the radiation fluxes are expressed in units of cal/cm^2·min and the albedo in units of %; R is the reflected radiation (emergent short-wavelength radiation), Q-R is the absorbed radiation and, T_r is the radiation temperature. Note: commas indicate decimal points.

A comparison of the observed and calculated average seasonal fields of the radiation balance and its components is of well-known interest. However, the difficulty of such a comparison consists in the fact that the calculated data with respect to the seasonal and monthly values of the radiation balance are descriptive mainly by the data on the emergent long-wavelength radiation. Therefore, it proved to be possible to carry out a comparison of the measured and calculated values only on a model of this component of the radiation

balance. The corresponding maps for all the seasons of the year are reproduced in detail in [60].

A comparison of the experimental average seasonal maps of the emergent long-wavelength radiation of the Earth-atmosphere system constructed on the basis of the data of [42] with the calculated climatological [45] maps reveals a clearly expressed qualitative agreement. On the basis of the data of the measurements and the calculations a decrease of the emergent radiation F_∞ with an increase in latitude is observed in all seasons of the year. In the winter the maximum values of F_∞ occur in the near-equatorial latitude and /51
have values which exceed somewhat 0.39 cal/cm^2·min. Minimum values of about 0.30 cal/cm^2·min are observed in the Southern Hemisphere, and 0.22 cal/cm^2·min in the Northern Hemisphere. The locations of the maxima obtained as a result of the calculations and the measurements agree well enough. All the minima are located in the near-equatorial zone. The most significant maxima ($F_\infty \geq 0.38$ cal/cm^2·min) occur in the Pacific Ocean over the Australian desert and partly over North and Central Africa and over South America.

The smallest deviations of the measured and calculated values of the emergent radiation in the winter (December, January, February) occur in the Northern Hemisphere. Here, the zonality of the field of emergent long-wavelength radiation is maintained to the greatest extent. We should note that the isolines of the measured values are smoother than the isolines of the calculated values. In the Northern Hemisphere the deviations of the calculated values of the emergent radiation from the measured values are comparatively small. In the Southern Hemisphere they are more significant.

A similar nature of the variations of the emergent radiation is observed during the spring and fall periods. In the summer the range of variation of the absolute values is somewhat smaller than in winter. The emergent radiation varies from 0.30 cal/cm^2·min (calculations) and 0.26 cal/cm^2·min (measurements) to 0.42 and 0.40 cal/cm^2·min, respectively. The quantitative agreement of the measured and calculated values is worse than in the winter-time. In comparison with the winter, the maxima are shifted somewhat to the north. The zonality is disrupted. Although the qualitative picture of the

geographical distribution of the emergent radiation on the basis of the data of measurements and calculations is very similar in the summer, a significant discrepancy is observed in the quantitative respect. The measured values exceed the calculated values almost everywhere.

Thus, a comparison of the calculated climatological seasonal maps of the emergent radiation of the Earth-atmosphere system with the map constructed on the basis of the data of measurements from satellites showed that, as a rule, the measured values exceed the calculated values in all seasons of the year. The smallest discrepancies are observed in the Northern Hemisphere in the winter and spring. In the spring in some regions of the Northern Hemisphere an increase occurs in the calculated values over the measured values. The results concerning the maps are valid for mean latitudinal values.

A comparison of the calculated values of the mean latitudinal profiles of the emergent radiation with the measured profiles showed (Table 4) that in all seasons of the year an increase of F_∞ is observed from the poles to the Equator. On the average the deviation between the calculated and measured values varies within the range from +0.01 to -0.03 cal/cm^2·min for specific latitudes.

Comparisons of the average values of the radiation balance and its components obtained by means of calculation and from measurements made by /52
the Kosmos-144 satellite have been carried out in the paper of L. V. Berkovich [59]. The data of an actinometric grid of stations for July 1967 were also used. This procedure permitted comparing the calculated values of the effective radiation of the Earth's surface, the emergent radiation, and the inflow of heat to the entire thickness of the atmosphere with the corresponding measured values. The average values of the emergent radiation amounted to 0.419 cal/cm^2·min and to 0.404 cal/cm^2·min on the basis of the data from the measurements.

L. N. D'yachenko and K. Ya. Kondrat'ev [56, 58], carrying out similar comparisons in 1966, obtained on the average, a value of F_∞ = 0.33 cal/cm^2·min on the basis of 89 calculated cases and F_∞ = 0.34 cal/cm^2·min on the basis of 74 cases of measured values (Tiros III).

Correlating the values F_∞ calculated according to K. Ya. Vinnikov's model with the values measured by the Tiros III satellite, the authors [58] obtained a linear dependence, although the correlation did not appear to be too high. A similar dependence was obtained upon the correlation of the values of the emergent radiation measured with the help of actinometric radiosondes and the calculated values for four points in the Soviet Union (Dolgoprudnyy, Vysokaya Dubrava, Kiev, and Tashkent). This dependence proved to be linear with the correlation coefficient r = 0.90.

TABLE 4

MEAN LATITUDINAL VALUES OF THE EMERGENT RADIATION OF THE EARTH-ATMOSPHERE SYSTEM FOR THE FOUR SEASONS OF THE YEAR ON THE BASIS OF DATA FROM CALCULATIONS AND MEASUREMENTS (cal/cm^2·min).

Latitude, Degrees	Winter		Spring		Summer		Fall	
	Calc.	Meas.	Calc.	Meas.	Calc.	Meas.	Calc.	Meas.
80--70 N.	0,231	0,20	0,249	0,24	0,285	0,29	0,255	0,25
70--60	0,262	0,24	0,279	0,26	0,294	0,31	0,276	0,27
60--50	0,268	0,26	0,282	0,28	0,299	0,33	0,284	0,30
50--40	0,282	0,27	0,293	0,30	0,315	0,35	0,303	0,33
40--30	0,300	0,31	0,313	0,32	0,340	0,36	0,313	0,35
30--20	0,311	0,35	0,348	0,36	0,358	0,36	0,357	0,37
20--10	0,351	0,37	0,344	0,42	0,321	0,35	0,339	0,37
10--0	0,339	0,36	0,335	0,36	0,320	0,34	0,329	0,37
0--10 S.	0,342	0,36	0,341	0,36	0,344	0,37	0,339	0,39
10--20	0,345	0,37	0,342	0,36	0,344	0,38	0,341	0,39
20--30	0,345	0,36	0,335	0,36	0,325	0,36	0,332	0,37
30--40	0,329	0,34	0,315	0,34	0,305	0,33	0,315	0,35
40--50	0,309	0,32	0,295	0,30	0,272	0,29	0,300	0,32
50--60	0,291	0,30	0,279	0,27	0,271	0,26	0,275	0,30
60--70		0,28		0,23		0,22		0,27
70--80		0,27		0,20		0,19		0,23
Earth as a Whole	0,32	0,32	0,32	0,33	0,33	0,33	0,33	0,34

Note: commas indicate decimal points.

Utilizing the Nimbus II data, E. Raschke and W. R. Bandeen [40] investigated the day-to-day variability of the planetary fields of albedo and emergent long-wavelength radiation, and they also carried out a statistical /53 reduction of the measurements' results with the purpose of constructing global maps of the dispersions of A and F_∞. Upon an analysis of these maps one's attention is drawn first of all to the fact that the field of the

dispersions is a graphic representation of the location of the main regions of the cyclonic activity and other synoptic features. Thus, for example, the albedo's dispersion reaches maximum values (12.5%) in a belt of the intertropical convergence zone. A large value of the dispersion of the albedo in the emergent radiation is observed in the southern part of the Pacific Ocean, which is known as a zone of high frequency of cyclones. A similar situation occurs in the North Atlantic (50-60° N. Lat.). On the contrary, small values of the dispersions are characteristic for extensive regions of the subtropics of both hemispheres. The day-to-day variability of the fields of the albedo and the emergent radiation is primarily determined by the effect of cloudiness.

Comparison with Data of Independent Measurements. Although the quality of the measurements has reached a sufficiently high level as the result of the improvement of satellite actinometric instrumentation, the problem of comparing the data of such measurements with the results of independent measurements carried out in particular from airplanes and balloons undoubtedly remains an urgent one. In order to achieve more successful interpretation of the data of satellite actinometric measurements, combined experiments which have as their purpose the accomplishment of simultaneous measurements of the radiation characteristics with the help of ground-based, airplane, balloon, and satellite instrumentation are particularly necessary [67-70]. Of course, comparison of heterogeneous (primarily from the point of view of spatial averaging) data represents a complicated problem. Therefore, the work carried out up to the present time is mainly of a systematic nature and does not offer possibilities for reliably controlling the quality of actinometric information.

Comparing the data of satellite measurements of the albedo with the results of balloon measurements is of interest. In Table 5 a summary is given of the albedo values quoted from K. Ya. Kondrat'ev, G. N. Gayevskaya, and G. A. Nikol'skiy's papers [66] and averaged over a small number (about 10) balloon ascents which were carried out in the summer and fall of 1962 under various meteorological conditions. The measurements were conducted in the /54

central part of the European territory of the USSR at a latitude of about 50° N. Lat.

TABLE 5

RESULTS OF BALLOON MEASUREMENTS OF THE EARTH-ATMOSPHERE'S ALBEDO

Month	No. of cases	A %
May	2	21.5
June	3	34.0
June	3	20.0
November	1	21.0
November (with snow)	1	62.0

A comparison of the data of Table 5 with the results of corresponding satellite measurements indicates a rather close agreement (unfortunately, correct quantitative agreement turns out to be impossible in the present case).

E. P. Barashkova, V. L. Hayevskiy, K. Ya. Kondrat'ev, and G. A. Nikol'skiy [67], continuing the experiment of comparing airplane, balloon, and satellite measurements of the radiation balance of its components, carried out a combined experiment on June 27, 1967, when at the instant of the Kosmos-156 satellite's passage over the city of Petrovsk (Privolzhskaya Mountain) ground--based airplane (at an altitude of 8.4 km), and balloon (at an altitude of 30 km) measurements of the radiation fluxes were also carried out. We will discuss the results of this experiment as given in [67].

At 6 hours 40 minutes Moscow time the airplane, balloon, and the Kosmos-156 meteorological satellite were located over the same point. For comparison nadir readings of the scanning devices made in the three spectral regions of 0.3-3, 3-30, 8-12 microns were used from the satellite data. The complexity of comparing the results of measurements corresponding to different altitudes consists in the fact that the areas viewed by the radiation receivers are different, and the underlying surface is nonuniform in the radiation sense. This situation makes the problem of the reduction of the averaging scales a difficult one to solve.

In Table 6 are indicated the radii r_1 (in km) of the circles corresponding to different view angles α and various altitudes H.

TABLE 6

GEOMETRY OF THE COMBINED EXPERIMENT

$\alpha°$	H km			
	10	20	30	600
4	0.349	0.698	1.045	20.94
6	0.524	1.048	1.572	31.44
140	27.47	54.94	82.41	1,648.2
180	385	544	667	2,982.2

Because of the Earth's curvature the radius of the area viewed at $\alpha = 180°$ is limited by the detection range, which was calculated from the equation $D = 3.85\sqrt{H}$, where H is in meters.

The area viewed by the satellite scanning receiver at the nadir amounts to $41.88 \times 62.9 = 2,634.25$ km^2. Approximately the same area is viewed by a receiver with a view angle of $\alpha = 140°$ from an altitude of H = 10.3 km (r = 29 km).

In the simplest case when the brightness of the underlying surface J is constant and the medium between the underlying surface and the radiation receiver is optically empty, the energy irradiance from a circle with a radius /55 of r of a horizontally-mounted detector with a view angle α and an area S_0 at an altitude of H is equal to

$$F = \pi J S_0 \frac{r^2}{H^2+r^2} = \pi J S_0 \sin^2 \frac{\alpha}{2} .$$

This relation permits one to estimate the contribution of circles of various radii to the total energy received. The radii r_2 (in km) of the circles which provide a contribution η equal to 0.5; 0.6; ...; 0.95 of the upward radiation flux at $\alpha = 180°$ are presented in Table 7.

TABLE 7

RADIATION FLUXES AND FIELDS OF VIEW

H km	η					
	0.5	0.6	0.7	0.8	0.9	0.95
8	8.0	9.8	12.2	15.8	23.7	33.8
10	10.8	12.2	15.2	19.8	29.6	42.2
20	19.9	24.3	30.3	39.3	58.1	82.3
30	29.7	36.3	45.3	58.6	86.3	120.3

A circle with a radius of r = 29.8 km, which corresponds in cross section to a rectangle viewed from the satellite, provides the following contribution to the upward radiation flux at an altitude of H:

H km . . .	5	10	15	20	25	30
η	0.97	0.89	0.79	0.68	0.58	0.48

In order to obtain values of η which correspond to actual conditions, it is necessary to have available data on the radiation's angular distribution at various altitudes.

We will compare the individual components of the radiation balance measured at various levels in the atmosphere. Stable anticyclonic weather was observed in the region of the comparisons. The Sun's altitude at the instant of comparison was 25°.

Total Radiation Q. Based on the data of ground-based stations the average value of the total radiation at 6 hours 30 minutes was 0.495 cal/cm^2··min for an average solar altitude of 22.6°. In order to reduce this value to $h_\odot$ = 25°, the equation $Q = \frac{S_0 \cos\theta}{1 + f\cos\theta}$ was used, where S_0 is the solar constant, θ is the zenith angle, and f is a coefficient characterizing the atmosphere's properties. For $h_\odot$, Q = 0.57 cal/cm^2·min is obtained.

For the satellite's altitude Q = S_0 sin $h_\odot$. Taking account of the correction for the Sun-Earth distance, we have S_0 = 1.91 cal/cm^2·min and sin $h_\odot$ = sin 25° = 0.423. Consequently, Q = 1.91 × 0.423 = 0.81 cal/cm^2·min.

Thus, the values of Q at various altitudes are as follows (Table 8):

TABLE 8 /56

TOTAL RADIATION

H km	Q cal/cm^2·min	ΔQ
0 (Earth)	0.57	0.10
8.4 (Airplane)	0.67	0.13
30 (Balloon)	0.80	0.01
600 (Satellite)	0.81	0.23
0-30		0.24
0-600		

Reflected Radiation R. Based on the data of ground-based observations the reflected radiation at 6 hours 30 minutes varies from 0.09 to 0.13 cal/cm^2·min. The average value is R = 0.11 cal/cm^2·min. Upon a change of the Sun's altitude from 22.5 to 25° the albedo of thick grain grass decreases by not more than 0.02 A, whereby

$$A_{h_\odot=25} = \frac{R}{Q_{h_\odot=22.5}}(1 - 0.02) = \frac{0.11}{0.50} \times 0.98 = 0.218.$$

Thus, $R_{h_\odot=25} = 0.57 \times 0.218 = 0.12$ cal/cm^2·min.

Measurements of the reflected radiation were carried out from an airplane with two instruments: a pyranometer and a wide-angle detector of the satellite actinometric instrumentation. The view angle of the latter instrumentation is equal to 140°. The instrument's readings are reduced to a view angle of 180° by the introduction of the factor 1/0.885.

The transition from the readings of the scanning instrument mounted on a satellite to the upward flux of short-wavelength radiation was carried out with the help of the scheme of K. Shifrin et al., [71]. On the basis of this scheme the following values of the upward flux of short-wavelength radiation (cal/cm^2·min) correspond to the nadir values of the intensity of reflected radiation J_r, which is equal to 0.03-0.04 cal/cm^2·min·ster for the Petrovsk region:

J_r	$h^\circ_\odot$			
	10	30	50	70
0,03	0,119	0,120	0,118	0,110
0,04	0,144	0,154	0,144	0,140

Therefore, we obtain for $h_\odot = 25°$:

J_r	R	πJ_r
0,03	0,12	0,09
0,04	0,15	0,12

A composite table of the values of R at various altitudes (km) has the following form: /57

H	R	R^*
0	0,12	0,10
8,4	0,15—0,16	0,18
30	0,165	—
600	0,12—0,15	0,20

Here, for comparison the values are also presented of R*, which are the results of the calculations of K. S. Shifrin and N. P. Pyatovskaya [72] for the standard radiative atmosphere (optical thickness of 0.3, horizontal range of visibility of 20 km, precipitable water content of 2.1 g/cm^2, and carbon dioxide gas content of 264 atm cm) and for grass cover. The values of R* for $h_\odot = 25°$ are obtained by interpolation of the data in Table 7.

The values of the emergent radiation derived with the help of K. S. Shifrin's scheme on the basis of satellite data seem somewhat underestimated, since in the first place the transition from H = 10 km to H = 600 km should be accompanied by some increase in R, and in the second place, it is difficult to expect any variation of the values of R above 30 km. The airplane and balloon measurements give consistent results.

Radiation Temperature. On the basis of the data of ground-based stations, the surface's temperature at 6 hours 30 minutes in the territory

within the range 50° N. Lat. $\leqslant \phi \leqslant$ 55° N. Lat. and 35° E. Long. $\leqslant \lambda \leqslant$ 50° E. Long. varied from 17 to 26° (the ground temperatures were 17 and 24° at the stations nearest to Petrovsk).

On the basis of airplane measurements, the radiation temperature T_r varied from 15 to 19°. A correction to the radiation temperature ΔT, introduced for the transition to the true surface temperature, varies from 6.5 to 8°.

A correction obtained by K. Ya. Kondrat'ev, E. P. Novosel'tsev, and N. E. Ter-Markaryants [73] for the Volgograd region on the basis of long-term average values of the temperature and the air's humidity in June was introduced to the radiation temperature measured from the satellite. In this case ΔT = 15°.

The values of the radiation temperature at various altitudes H km are presented in the following table:

H	T_r	ΔT	$T_r + \Delta T$
0	17—26	0	17—26
10	15—20	6—8	21—88
30	—	—	—
600	8—11	15	23—26

Taking into account the comparatively low accuracy of a surface measurement temperature, one can consider the values of the temperature obtained after the introduction of the corrections to be rather close. /58

Upward Long-Wavelength Radiation $\dot{F}_i^{\uparrow}$. The ground-based grid of station does not give data on the long-wavelength fluxes $F_L^{\uparrow}$. However, it follows from the special measurements carried out earlier but on the average $F_L^{\uparrow} = \sigma T_0^4$, where T_0 is the temperature of the underlying surface. $F_L^{\uparrow}$ varies from 0.58 to 0.65 cal/cm^2·min, in agreement with the temperature of the level of the underlying surface.

On the basis of the airplane measurements in the Petrovsk region at an altitude of 8.4 km with the help of the instruments mentioned, the following values were obtained for the upward flux of long-wavelength radiation in units of cal/cm^2·min:

Type of instrument	View angle, °	
	140	180
Wide-angle.	0.410	0.465
Scanning.	0.425	0.480
Meteorological Radiometer . .	0.418	0.474
Average	0.418	0.473

The factor 1/0.885 was introduced for the transition to a view angle of 180°.

On the basis of the data of the balloon measurements at an altitude of 8.4 km, the upward flux of long-wavelength radiation is equal to 0.363 cal/cm^2·min.

The discrepancy of the values of $F_L^{\uparrow}$ measured from the airplane and the balloon amounts to about 28%. Such a discrepancy is caused primarily by the comparatively low accuracy of the measurements; the difference in the time at which the measurements were made (90 min) is probably another reason for the discrepancy. The accuracy of the measurements by the airplane instruments is about 8%; the errors of the measurements by the balloon instruments do not exceed 5% in the troposphere and 11% in the stratosphere.

The flux of radiation for H = 600 km is calculated as $F_L^{\uparrow} = \pi J_L$, where J_L is the brightness at the nadir on the basis of the data for measurements from the satellite. The results of a comparison of the fluxes $F_L^{\uparrow}$ measured at various altitudes are presented in Table 9.

/59

TABLE 9

UPWARD LONG-WAVELENGTH RADIATION (cal/cm^2·min)

H km	Ground-based, airplane, and satellite measurements	Balloon measurements	Calculated data
0	0.58-0.65	0.58	0.53
8.4	0.47	0.36	0.37
30	--	0.41	0.34
50	--	--	0.35
600	0.41	--	--

The results of the calculations of Kondrat'ev and Niylisk [74] for the standard atmosphere are presented in this same table.

In order to obtain reliable results for the comparison of the values of $F_L^{\uparrow}$ at various levels, we should carry out simultaneous measurements with the different instruments at one and the same level; this procedure permits obtaining a clearer idea as to the effect of the measurement errors.

It is natural that the first attempt at synchronous investigation of the three-dimensional structure of the radiation field in the atmosphere with the help of instrumentation mounted on airplanes, balloons, and satellites, in combination with the data of a ground-based grid of actinometric stations, gave results which are useful from the point of view of the rational planning of subsequent investigations. As should have been expected, the deviations of the results from the measurements of the upward long-wavelength radiation fluxes turned out to be significant, which once more emphasizes the urgency of the problem of increasing the accuracy of thermal radiation measurements. The agreement of the data from the measurements of short-wavelength radiation ought to be considered unexpectedly good: the multiplicity of sources of errors not taken into account has prompted the expectation of significantly poorer agreement. It is indisputable that the carrying out of a combined experiment with the application of well-studied and unified instrumentation is a problem for further work. The improvement of the procedure for reducing the data from satellite measurements (a scheme for the conversion from the readings of detectors with a restricted view angle to hemispherical radiation fluxes) and attentive study of the problem of the averaging scales have important meaning. The simultaneous execution of measurements of the angular and spectral distribution of the radiation have exceptionally important meaning for the correct interpretation of the results obtained and for a more complete specification of the radiation field. This situation permits making further steps toward the realization of a combined radiation experiment [67-70].

The Solar Constant. Since only short-wavelength radiation reflected by the Earth into space is measured from satellites, the problem of the solar

constant acquires fundamental meaning for determining the albedo and the absorbed radiation. Until recent times the value for the solar constant of 2.00 cal/cm^2·min has been considered to be generally accepted. However, measurements carried out during recent years [75, 76], and in particular the balloon measurements of the solar radiation made for many years by workers at Leningrad University [76, 83], have shown that the actual value of the solar constant is about 1.94 cal/cm^2·min. According to [76], this value is the maximum possible and is observed when the Wolf numbers are of the order of 80-100. As the Wolf number varies (in the direction of an increase /60 or a decrease), the solar constant decreases, and the maximum decrease reaches 2-2.5%. If this result is confirmed by the data of direct satellite measurements (and there is significant necessity of this), it is evident that the necessity arises of completing a program of satellite actinometric measurements and carrying out continuous measurements of the solar constant for the purpose of monitoring its variation.

REFERENCES

1. Kondrat'ev, K. Ya., *Meteorologicheskiye Sputniki* [Meteorological Satellites], Leningrad, "Gidrometeoizdat" Press, 1963. /60
2. Kondrat'ev, K. Ya., E. P. Vorisenkov and A. A. Morozkin, *Prakticheskoye Ispol'zovaniye Dannykh Meteorologicheskikh Sputnikov* [Practical Utilization of the Data of Meteorological Satellites], Leningrad, "Gidrometeoizdat" Press, 1966.
3. Kondrat'ev, K. Ya., E. P. Vorisenkov and A. A. Morozkin, *Pole Izlucheniya Zemli Kak Planety* [The Radiation Field of the Earth as a Planet], Leningrad, "Gidrometeoizdat" Press, 1967.
4. Kondrat'ev, K. Ya. and Yu. M. Timofeyev, *Termicheskoye Zondirovaniye Atmosfery pri Pomoschi Sputnikov* [Thermal Sounding of the Atmosphere with the Help of Satellites], Leningrad, "Gidrometeoizdat" Press, 1970.
5. Basharinov, A. Ye., A. S. Gurvich and S. T. Yegorov, "Determination of Geophysical Parameters from Measurements of Thermal Radio Emission by the Kosmos-243 Artificial Earth Satellite," *Doklady Akademii Nauk SSSR*, Vol. 188, No. 6, 1968.
6. Obukhov, A. M. and M. S. Tatarskaya, "Field of the Integral Moisture--Containing Atmosphere Over the Southern Hemisphere on the Basis of Measurements of the Thermal Radio Emission by the Kosmos-243 Staellite," *Meteorologiya i Gidrologiya*, No. 11, 1969.
7. Minina, L. S., *Praktika Nefanaliza* [The Practice of Nephanalysis], Leningrad, "Gidrometeoizdat" Press, 1970.
8. Sonechkin, D. M., "Classification of the Types of Television Images of Cloudiness and the Earth's Surfaces Obtained from a Satellite in an Experimental System," *Meteorologiya i Gidrologiya*, No. 9, 1968.
9. Popova, T. P. et al., "Characteristics of the Cloudiness Over the Northern Hemisphere in the Summer of 1965 on the Basis of Data from a Meteorological Satellite," *Trudy GMTs*, No. 11, 1967.
10. Johnson, A. W., "Weather Satellites: II," *Scientific American*, Vol. 220, No. 1, 1969.
11. Booth, A. L. and V. R. Taylor, "Mesoscale Archive and Products of Digitized Video Data from ESSA Satellites," *ESSA Techn. Memo., NESCTM 9*, October 1968.
12. McClain, E. P. and D. R. Baker, "Experimental Large-Scale Snow and Ice Mapping with Composite Minimum Brightness Charts," *ESSA Techn. Memo., NESCTM 12*, September 1969.
13. McClain, E. P., "Application of Environmental Satellite Data to Oceanography and Hydrology," *ESSA Techn. Memo., NESCTM 19*, January 1970.
14. Vonder Haar, T. H., "Meteorological Applications of Reflected Radiance Measurements from ATS-1 and ATS-III," *J. Geophys. Res.*, Vol. 74, No. 23, 1969.
15. Doolittle, R. C., C. L. Bristor and L. Lauritson, "Mapping of Geostationary Satellite Pictures: An Operational Experiment," *ESSA Techn. Memo., NESCTM 20*, March 1970.

16. Fujita, T. T., K. Watanabe and T. Izawa, "Formation and Structure of Equatorial Anticyclones Caused by Large-Scale Cross-Equatorial Flows Determined by ATS-1 Photographs," *J. Appl. Meteorol.*, Vol. 8, No. 4, 1969.
17. Anekeyeva, A. A., "Investigation of Data on Cloudiness Obtained with the Help of Artificial Earth Satellites in an Objective Analysis of the Wind Field," *Trudy GMTs*, No. 36, 1968.
18. Kanaskova, I. Ya. and M. S. Purganskiy, "Determination of the Wind Velocity in a Large-Scale Atmospheric Vortex from the Cloudiness Data Arriving from an Artificial Earth Satellite," *Meteorologiya i Gidrologiya*, No. 7, 1970.
19. Novak, Ch. S., "Deriving Upper Tropospheric Winds by Computer from Single Image, Digital Satellite Data," *ESSA Techn. Memo., NESCTM 13*, June 1969. /61
20. Musayelyan, Sh. A., "Some Problems of the Miracle Interpretation of Cloudiness Information Arriving from Artificial Earth Satellites," *Trudy GGO*, No. 166, 1964.
21. Musayelyan, Sh. A. and L. V. Belinskaya, "Establishing the Fields of Meteorological Elements from Data of Observations from Satellites," *Trudy GMTs*, No. 30, 1968.
22. Barret, E. C., "The Estimation of Monthly Rainfall from Satellite Data," *Month. Weath. Rev.*, Vol. 98, No. 4, 1970.
23. Warnecke, G., "The Remote Sensing of Stratospheric Temperatures and Some Results from the Nimbus II Satellite Experiment," *Goddard Spaceflight Center, X-622-67-471*, September 1967.
24. Warnecke, G. and A. McCulloch, "Stratospheric Temperature Pattern Derived from Nimbus II Measurements," *Goddard Spaceflight Center, X-622-67-436*, August 1967.
25. Kennedy, J. S., "An Atlas of Stratospheric Mean Isotherms Derived from Tiros VII Observations," *Goddard Spaceflight Center, X-622-66-307*, July 1966.
26. Gayevskiy, V. L. et al., "Meteorological Interpretation of Infrared Images of the Earth from Space," *Meteorologiya i Gidrologiya*, No. 4, 1968.
27. Gayevskiy, V. L. et al., "Problems of the Meteorological Interpretation of Infrared Images of the Earth from Space," in the book: *Aktinometriya i Optika Atmosfery* [Actinometry and Atmospheric Optics], Leningrad, Gidrometeoizdat Press, 1969.
28. Nordberg, W., "Geophysical Observations from Nimbus I," *Science*, Vol. 150, No. 3696, 1965.
29. Barnes, J. C., D. T. Chang and J. H. Willard, "Satellite Infrared Observation of Arctic Sea Ice," *AIAA Paper No. 301*, 1970.
30. Rao, P. K., W. R. Curtis, A. E. Strong and E. P. McClain, "Remote Sensing of Sea Surface Temperature," *Proc. Sixth Space Congr.*, Cocoa Beach, Fla., Vol. II. Session 5, pp. 5-10, March 17-19, 1969.
31. Zhvalev, V. F., K. Ya. Kondrat'ev and N. Ye. Ter-Markaryants, "The Possibility of Using Infrared Images of the Earth for Tracing the Dynamics of C-Currents and for Discovering Jet Streams and Noctilucent Clouds," *Izvestiya AN SSSR, Ser. Fiz. Atm. i Okeana*, Vol. III, No. 11, 1967.

32. Oliver, V. J., "Some Applications of Space Observations to Meteorology, Oceanography and Hydrology," Preprint. Anaheim, California, October 1967.
33. Warnecke, G., L. M. McMillin and L. J. Allison, "Ocean Current and Sea Surface Temperature Observations from Meteorological Satellites," *NASA Techn. Note D-5142*, Goddard Spaceflight Center, November 1969.
34. McClain, E. P., "Applications of Environmental Satellite Data to Oceanography and Hydrology," *ESSA Techn. Memo., NESCTM 19*, January 1970.
35. Arking, A., "The Latitudinal Distribution of Cloud Cover from Tiros Photographs," *Science*, Vol. 143, pp. 569-572, 1964.
36. Clapp, P. F., "Global Cloud Cover for Seasons Using 'Tiros' Nephanalaysis," *Month. Weath. Rev.*, Vol. 92, pp. 495-507, 1964.
37. Winston, J. S., "Global Distribution of Cloudiness and Radiation as Measured from Weather Satellites," *Climate of the Free Atmosphere*, Chapter 6, Amsterdam, Elsevier Press, 1969.
38. Kornfield, J., A. F. Hasler, K. J. Hanson and V. E. Suomi, "Photographic Cloud Climatology from ESSA III and V Computer-Produced Mosaics," *Bull. Amer. Met. Soc.*, Vol. 48, No. 12, 1967.
39. Raschke, E., "The Radiation Balance of the Earth-Atmosphere System from Radiation Measurements of the Nimbus II Meteorological Satellite," *NASA Techn. Note D-4589*, July 1968.
40. Raschke, E. and W. R. Bandeen, "The Radiation Balance of the Planet Earth from Radiation Measurements of Satellite Nimbus II," *J. Appl. Met.*, Vol. 9, No. 2, 1970.
41. Raschke, E., T. H. Vonder Haar, W. R. Bandeen and M. Pasternak, "The Radiation Balance of the Earth-Atmosphere System During June and July 1969 from Nimbus III Radiation Measurements — Some Preliminary Results," *COSPAR XIII Symposium on Remote Sounding of the Atmosphere*, Leningrad, May 1970.
42. Vonder Haar, T. H., "Variations of the Earth's Radiation Budget," *The Univ. of Wisconsin Contr. NASW-65*, February 1968.
43. Vonder Haar, T. H. and V. E. Suomi, "Satellite Observations of the Earth's Radiation Budget," *Science*, No. 3868, February 1969.
44. Vonder Haar, T. H. and V. E. Suomi, "Measurements of the Earth's Radiation Budget from Satellites During a Five-Year Period," *J. Atm. Sci.*, Vol. 27, No. 5, 1970.
45. Kondrat'ev, K. Ya., L. N. D'yachenko and K. Ya. Vinnikov, "The Climatology of the Earth's Radiation Balance in its Contemporary Stage," *Problemy Fiziki Atmosphery*, No. 7, 1969.
46. Vinnikov, K. Ya., "The Problem of Interpreting the Results of Measurements of the Emergent Radiation by Radiometers with a Restricted Field of View Mounted on Meteorological Earth Satellites," *Trudy GGO*, No. 228, 1968.
47. Kagan, R. L., "Some Problems of the Interpretation of Precipitation Gauge Data," *Trudy GGO*, No. 208, 1967.
48. Vinnikov, K. Ya., "The Problem of an Objective Analysis of the Fields of Actinometric Quantities," *Trudy GGO*, No. 208, 1967.

49. Kondrat'ev, K. Ya. and L. N. D'yachenko, "A Comparison of Experimental and Calculated Climatological Maps of the Mean and Radiational Balance of the Earth and Its Components," *Trudy GGO*, No. 235, 1970.
50. Kondrat'ev, K. Ya. and L. N. D'yachenko, "A Comparison of the Results of Calculations of the Emergent Radiation with the Data of Measurement Made With the Help of Actinometric Radiosondes and Meteorological Satellites," *Trudy GGO*, No. 203, 1967.
51. Berlyand, T. G., "Thermal Balance of the Atmosphere of the Northern Hemisphere," in the book: *A. I. Voyeykov i Problemy Sovremennoy Klimatologii* [A. I. Voyeykov and Problems of Contemporary Climatology], Leningrad, Gidrometeoizdat Press, 1956.
52. Vinnikov, K. Ya., "Emergent Radiation of the Earth-Atmosphere System," *Trudy GGO*, No. 168, 1965.
53. Vinnikov, K. Ya., "The Albedo of the Earth-Atmosphere System and the Field of Emergent Short-Wavelength Radiation," *Trudy GGO*, No. 170, 1965.
54. Katayama, A., "On the Radiation Budget of the Northern Hemisphere. II. Hemispheric Distribution. III. Zonal Cross Section and Energy Consideration," *J. Met. Soc. Japan*, Ser. II, Vol. 45, No. 1, February 1967.
55. London, J. and T. Sasamori, "Radiative Energy Budget of the Atmosphere," *COSPAR XIII Symposium on Remote Sounding of the Atmosphere*, Leningrad, May 1970.
56. D'yachenko, L. N. and K. Ya. Kondrat'ev, "Distribution of the Long-Wavelength Balance Over the Earth," *Trudy GGO*, No. 170, 1965.
57. Sabatini, R. R. and V. E. Suomi, "On the Possibility of Infrared Cooling Estimates from Satellite Observations," *J. Atm. Sci.*, Vol. 19, No. 4, 1962.
58. Kondrat'ev, K. Ya. and L. N. D'yachenko, "Correlation Relations Between Values of the Atmosphere's Long-Wavelength Balance from the Emergent Radiation," *Trudy GGO*, No. 184, 1966.
59. Berkovich, L. V., "Radiation Fluxes and Heat Input to the Atmosphere on the Basis of Empirical and Calculated Data," *Trudy GMTs*, No. 50, 1969.
60. Kondrat'ev, K. Ya. and L. N. D'yachenko, "A Comparison of Experimental and Calculated Values of the Emergent Long-Wavelength Radiation for Various Seasons of the Year," *Trudy GGO*, No. 242, 1970.
61. Kondrat'ev, K. Ya., "Radiation in the Atmosphere," New York, Acad. Press, 1969.
62. "Tiros II Radiation Data User's Manual," *Goddard Spaceflight Center*, 1961.
63. Borisenkov, E. P., Yu. P. Doronin and K. Ya. Kondrat'ev, "Structural Characteristics of the Radiation Field of the Earth as a Planet," *Kosmicheskiye Issledovaniya*, Vol. 1, No. 1, 1963.
64. Borisenkov, E. P., Yu. P. Doronin and K. Ya. Kondrat'ev, "Structural Characteristics of the Fields of Emergent Radiation on the Basis of the Interpretation," *Kosmicheskiye Issledovaniya*, Vol. 3, No. 3, 1965.
65. Gandin, L. S. and V. P. Boltenkov, "A Procedure for the Objective Analysis of Actinometric Information from Meteorological Earth Satellites," *Trudy GGO*, No. 166, 1964.

"The aeronautical and space activities of the United States shall be conducted so as to contribute . . . to the expansion of human knowledge of phenomena in the atmosphere and space. The Administration shall provide for the widest practicable and appropriate dissemination of information concerning its activities and the results thereof."

— NATIONAL AERONAUTICS AND SPACE ACT OF 1958

NASA SCIENTIFIC AND TECHNICAL PUBLICATIONS

TECHNICAL REPORTS: Scientific and technical information considered important, complete, and a lasting contribution to existing knowledge.

TECHNICAL NOTES: Information less broad in scope but nevertheless of importance as a contribution to existing knowledge.

TECHNICAL MEMORANDUMS: Information receiving limited distribution because of preliminary data, security classification, or other reasons.

CONTRACTOR REPORTS: Scientific and technical information generated under a NASA contract or grant and considered an important contribution to existing knowledge.

TECHNICAL TRANSLATIONS: Information published in a foreign language considered to merit NASA distribution in English.

SPECIAL PUBLICATIONS: Information derived from or of value to NASA activities. Publications include conference proceedings, monographs, data compilations, handbooks, sourcebooks, and special bibliographies.

TECHNOLOGY UTILIZATION PUBLICATIONS: Information on technology used by NASA that may be of particular interest in commercial and other non-aerospace applications. Publications include Tech Briefs, Technology Utilization Reports and Technology Surveys.

Details on the availability of these publications may be obtained from:

SCIENTIFIC AND TECHNICAL INFORMATION OFFICE

NATIONAL AERONAUTICS AND SPACE ADMINISTRATION

Washington, D.C. 20546